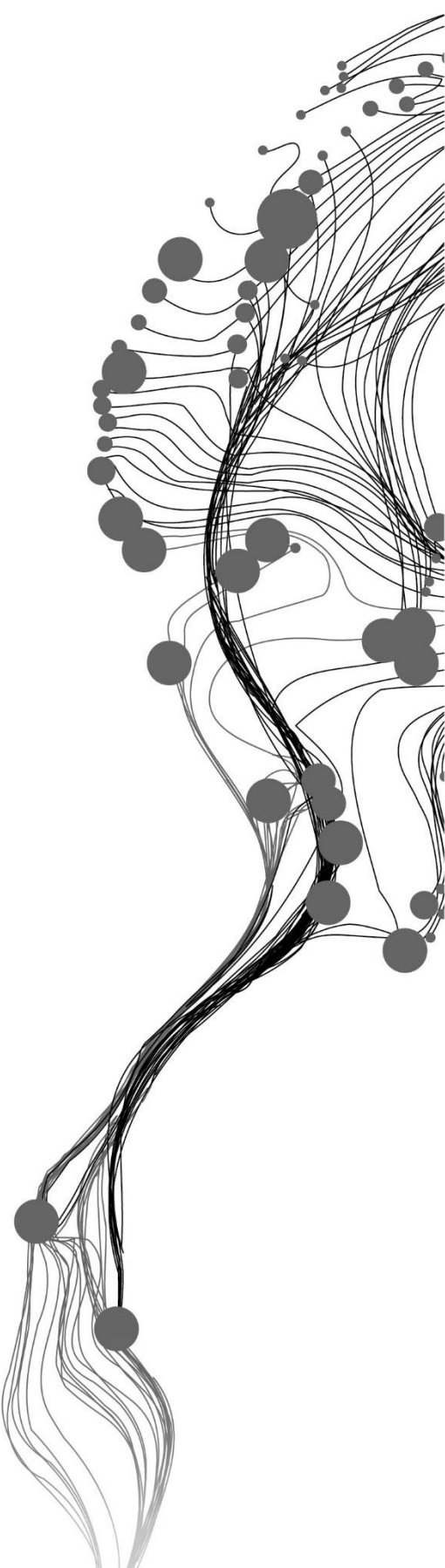


**EFFECT OF LAND COVER CHANGE
ON WATER BALANCE
COMPONENTS IN GILGEL ABAY
CATCHMENT USING SWAT MODEL**

HADILAWIT TADESSE AGA
March 2019

SUPERVISORS:
Dr. Ing. T.H.M. Rientjes
Ir. G.N. Parodi



EFFECT OF LAND COVER CHANGE ON WATER BALANCE COMPONENTS IN GILGEL ABAY CATCHMENT USING SWAT MODEL

HADILAWIT TADESSE AGA

Enschede, The Netherlands, March 2019

Thesis submitted to the Faculty of Geo-Information Science and Earth Observation of the University of Twente in partial fulfilment of the requirements for the degree of Master of Science in Geo-information Science and Earth Observation.

Specialization: Water Resources and Environmental Management

SUPERVISORS:

Dr. Ing. T.H.M. Rientjes

Ir. G.N. Parodi

THESIS ASSESSMENT BOARD:

Dr. M.W. Lubczynski (Chair)

Prof. Dr. Paolo Reggiani University of Siegen, Germany (External Examiner)

DISCLAIMER

This document describes work undertaken as part of a programme of study at the Faculty of Geo-Information Science and Earth Observation of the University of Twente. All views and opinions expressed therein remain the sole responsibility of the author and do not necessarily represent those of the Faculty.

ABSTRACT

Understanding effect of land cover (LC) change on water balance components is important for water resources planning and management. This study examines the effect of the land cover change on water balance components that include streamflow and actual evapotranspiration in Gilgel Abay catchment, Ethiopia. Five land cover maps of 1986, 2001, 2008, 2013 and 2018 are prepared and are used as input for Soil Water Assessment Tool (SWAT) model approach. Model simulation periods cover five windows that are a baseline (BL) and four altered periods (AP): 1986-1994 (BL), and altered periods including 1995-2001 (AP1), 2002 – 2008 (AP2), 2009- 2013 (AP3) and 2014 -2016 (AP4). SWAT is calibrated for the baseline period and optimized SWAT-model parameter set served for simulation for the subsequent four altered periods under two LC scenarios, with and with LC update. Land cover classification relied on supervised classification. Classification results are satisfying with Kappa coefficient that ranges between 0.75-0.81. The land cover change analysis shows that for the assessment period 1986-2018, that agricultural and residential area increased by 10.74% and 4.1% respectively; bare land and grassland decreased by 19.3% and 2.9% respectively. In the same period, forest and wetland values do not show clear increasing or decreasing trend: forest and wetland covered 8.44 % and 0.45% in 1986, 12.86% and 0.24% in 2001, 7.57% and 0.47% in 2008, 17.33% and 0.35% in 2013 and 15.88% and 0.40% in 2018 respectively. The SWAT model was calibrated using monthly streamflow at Wetet Abay gauging station. The model shows good performance with Nash Sutcliffe Efficiency (NSE) of 0.83. The model simulation assessment at Wetet Abay gauging station in AP1 to AP4 show good performance with NSE of 0.78 to 0.69 with LC update and deteriorated performance with NSE of 0.75 to 0.28 without LC update. The effect of LC changes on water balance components at the Gilgel Abay outlet to Lake Tana shows the runoff coefficient at annual base decreased from 56% in BL to 49% in AP4; while such coefficient calculated for evapotranspiration (i.e. $\sum \text{evapotranspiration} / \sum \text{precipitation}$) increased from 40% in BL to 49% in AP4; surface runoff/total discharge increased from 38% in BL to 49% in BL; and base flow/total discharge decreased from 62% in BL to 0.51% in AP4. 86% of the change in streamflow is attributed to LC change while the remaining 14% is attributed to climate change. This study also shows that for the assessment period effects of climate change on the hydrology of the Gilgel Abay basin are less prominent than effects by land use changes. Regardless of the limitation the study is relevant for sustainable water and environmental planning whereby planners and decision-makers can use.

Keywords: Gilgel Abay catchment, Land Cover, water balance components, SWAT Model.

ACKNOWLEDGEMENTS

I would like to thank Almighty GOD for his guidance and grace upon me and for giving me the courage, wisdom and strength to walk unpaved way to reach this point in life during all my works. I would like to express my sincere gratitude Netherlands Fellowship Programmes (NFP). I am grateful to Ministry of Water Irrigation and electricity, National Metrological Service Agency and Mapping agency of Ethiopia for giving me the necessary data which was helpful to accomplish this thesis work.

My thanks and warm feeling of appreciation to Dr. Ing. Tom Rientjes for his precious advice, encouragement and decisive comment during the research period. I would also like to say thanks my second supervisor Ir. Gabriel Parodi for his guidance and assistance for the accomplishment of this study. My special and genuine thanks also go to Dr. Abebe Demise Chukalla for his uninterrupted assistance, professional advice, co-operation and valuable comments and advices during my study.

I would also like to express my sincere thanks to Mekuanent Muluneh for his critical comments, fruitful suggestion and follow ups helped me to take this research in the right direction. Last but not least I would like to give my deepest appreciations and acknowledgements to my family, specially to my brother Musiker Tadesse for his appreciation, supports and encouragements.

TABLE OF CONTENTS

1.	Introduction.....	1
1.1.	Background	1
1.2.	Problem statement	1
1.3.	Significance of the study	2
1.4.	Research objective and questions	2
1.5.	Hypothesis of the study.....	2
2.	Literature review	5
2.1.	Land cover change	5
2.2.	Effects of land cover changes on hydrological processes	5
2.3.	Hydrological model.....	6
3.	Materials and Methods.....	11
3.1.	Study area and data.....	11
3.2.	Methods	18
3.3.	Attribution of change in streamflow to land cover change and climate change	30
4.	Results.....	33
4.1.	Land cover classification	33
4.2.	Calibration of the SWAT model.....	37
4.3.	Performance of the model with and without LC update	39
4.4.	Effect of land cover change on water balance component	43
4.5.	Attribution of change in streamflow to land cover change and climate change	44
5.	Discussion.....	46
6.	Conclusion	49

LIST OF FIGURES

Figure 1: Hypothetical scenarios to test NSE for model simulation with/without LC change adapted from Marhaento et al. (2017).....	3
Figure 2: The study area.....	12
Figure 3: Soil map of the study area.....	13
Figure 4: DEM of Gilgel Abay catchment.....	14
Figure 5: Ground control points (GCP) from google earth and from field data.....	15
Figure 6: Gauged station (Wetet Abay) and ungauged outlet.	16
Figure 7: Mean annual rainfall of metrological stations in Gilgel Abay catchment.....	17
Figure 8: Relationship of elevation versus mean annual rainfall of the metrological stations in Gilgel Abay catchment.	17
Figure 9: Map of weather stations in the catchment	18
Figure 10: The Methodology of the study.....	20
Figure 11: Flowchart showing steps on how to produce the Land cover map.....	24
Figure 12: SWAT model structure representation adapted from (Mekonnen et al., 2018).....	26
Figure 13: Gilgel Abay sub-basins, reaches.....	27
Figure 14: Framework to illustrate a fraction of excess water and energy adapted (Marhaento 2018).....	31
Figure 15: Land cover map of Gilgel Abay catchment for 1986, 2001, 2008, 2013 and 2018	33
Figure 16: Land cover of Gilgel Abay catchment in % (a) and km ² (b).....	35
Figure 17: Simulated hydrograph of the base period	38
Figure 18: Figure 14: Model performance, Nash-Sutcliffe efficiency with and without LC changes.....	39
Figure 19: Hydrograph of observed and simulated discharge with and without the land cover update for the altered period 1, 2, 3 and 4.....	40
Figure 20: Hydrograph of observed and simulated discharge with land cover update for the altered period 1, 2, 3 and 4.	41
Figure 21: Water balance components: (a) runoff coefficient and ET/P and (b) Qs/Q, Ql/Q and Qb/Q	44
Figure 22: Change of excess water and excess energy in relative to long term aridity index line.....	45
Figure 23: The ratio of water balance components in baseline and altered periods	47
Figure 24: Representation of SWAT model for water balance.....	54
Figure 25: Daily rainfall foreach stations.....	54

LIST OF TABLES

Table 1: Types of hydrological models adapted from (Tegegne et al. 2017)	7
Table 2: Model performance rating criteria, source from (Moriassi et al., 2007).....	9
Table 3: Climate classification in Ethiopia (source: (NMSA, 2001).	11
Table 4: Description of Landsat images	14
Table 5: Coordinates and elevation of the metrological stations in Gilgal Abay catchment.....	17
Table 6: Merging of land cover maps 2008 and 2013.....	22
Table 7: Shows the range of kappa coefficient and their interpretation adapted from Landis and Koch (1977)	25
Table 8: List of Parameters and their ranksss based on t-stat and p-values from SWAT cup.....	28
Table 9. Representation of calibration without land cover change	29
Table 10. Representation of calibration with land cover change	29
Table 11: Summary of the land cover percentage of Gilgel Abay watershed	34
Table 12: change detection of land cover maps	34
Table 13: confusion matrix accuracy for the classified image (1986).....	36
Table 14: confusion matrix accuracy for the classified image 2001.....	36
Table 15: confusion matrix accuracy for the classified image 2008.....	36
Table 16: confusion matrix accuracy for the classified image 2013.....	37
Table 17: confusion matrix accuracy for the classified image 2018.....	37
Table 18: Kappa coefficient values	37
Table 19: Summary of the calibrated value of flow parameters.....	39
Table 20: Mean annual water balance components in (mm)	43
Table 21: Summary of water balance components ratio in percentage	43
Table 22: Measure of the attribution streamflow alteration to LC change and climate change	45

1. INTRODUCTION

1.1. Background

Riebsame et al. (1994) refer to Land cover (LC) as the biophysical state of the earth's land surface and immediate sub-surface including biota, soil, topography, surface and groundwater, and human structures. According to Meyer et al. (1995), every parcel of land on the Earth's surface is unique in the cover it possesses. As such they categorise land cover as cropland, forest, wetland, pasture, roads, and urban areas among others (Meyer 1995). LC are distinct yet closely linked characteristics of the Earth's surface. Human activities are the major factors that largely determine the changes in land cover: agriculture, deforestation, and construction leave large areas of soil uncovered and unprotected, leading to high runoff (Quilbé et al. 2008). Large changes in land cover commonly have a significant effect on hydrologic characteristics of the soil, which consequently influence evapotranspiration and streamflow (Fonji and Taff 2014).

LC directly impacts the amount of evaporation, groundwater infiltration and overland runoff that occurs during and after precipitation events. Land cover change alters both runoff behaviour and the balance that exists between evaporation, groundwater recharge and stream discharge in specific areas and entire watersheds, with considerable consequence for all water users (Eshleman, 2004). Many studies have been carried out to evaluate the impacts of LC on water resources (Mango et al., 2011; Marhaento et al., 2017). These researches indicate that LC affect hydrological processes such as evapotranspiration, interception and infiltration, resulting in spatial and temporal alterations of surface and subsurface flows patterns.

The Gilgel Abay catchment is the largest catchment in the Lake Tana basin that discharges flows to the lake. According to (Kebede, 2009) the catchment is densely populated with an annual population growth rate of 2.31%. Thus, the effects of human activities such as deforestation, overgrazing and the expansion of the residential and agricultural areas increasingly alter the water balance components. Thus, quantifying water balance components and their changes as a consequence of land cover changes is important for water resources planning and management (Setegn et al., 2008). Examples are in flood control, hydrological drought, and water use. Impacts assessments commonly rely on hydrological modelling such as practices with the Soil Water Assessment Tool (SWAT) model that targets simulation of respective flow processes and water balance components.

1.2. Problem statement

Researches on the effect of land cover change on water balance components, which is relevant for water resources planning and management in Gilgel Abay, are limited and partial. Gumindoga et al. (2014) studied the effect of land cover change on streamflow for the year 1974, 1986, 2001 using TOPMODEL. Understanding the up to date land cover change and its effect on water balance components are important as the pressure on water rises and a comprehensive water resource management is required. A major problem in land cover change studies is that assessed findings on hydrological impacts are not always directly comparable with hydrological model assessments at very local scale (< 10 km²) over very short time periods (<15 years) as compared to long term (e.g. > 25 years) statistical time series analysis on streamflow for large basins. Although hydrological impacts result from land cover changes, for many basins magnitudes of impacts remain uncertain, this also since changes in hydrological processes could intensify runoff behaviour.

1.3. Significance of the study

This research aims at examining the effect of land cover on the rainfall-runoff, rainfall - ET relationship and streamflow response of the Gilgel Abay catchment. The research findings support decision makers in planning land cover and other development activities in a way to improve water resources planning and utilisation. This study extends and fills research gaps in the previous studies in the Gilgel Abay catchment with a focus on land cover change assessments. This study extends the period of past land cover change assessments to the year 2018 and employs distributed modelling to assess contributions of rainfall to streamflow and actual evapotranspiration

1.4. Research objective and questions

1.4.1. Objectives

General objective

To assess the effects of land cover change on water balance components in the Gilgel Abay catchment for five windows that cover for a baseline period:1986-1994 and altered periods (AP): 1995-2001 (AP1), 2002-2008 (AP2), 2008-2013 (AP3) and 2014-2018 (AP4).

Specific objectives

- I) To define and assess land cover changes over the sequential time periods.
- II) To parametrize the SWAT model for the baseline period and assess impacts by LC changes for altered periods.
- III) To quantify the contribution of the effects of land cover change and climate change on changes in streamflow and actual evapotranspiration.

1.4.2. Research questions

General research question

What are the effects of the land cover changes on water balance components in the Gilgel Abay catchment?

Specific research questions

- I) What are the land cover changes in Gilgel Abay catchment from 1986 to 2018?
- II) What are the optimized parameters of the SWAT model for the baseline periods and how do parameters affect simulation results for altered periods with LC changes and without LC changes?
- III) What are the contribution of land cover change and climate change on changes in streamflow and actual evapotranspiration?

1.5. Hypothesis of the study

To answer these research questions in this study, the SWAT model is applied for five-time windows. These five-time windows are baseline period, i.e., 1986 to 1994, and four altered periods, i.e., 1995-2001, 2002 - 2008, 2009- 2013 and 2014 -2018. The base period is used for model calibration and the altered periods are used to assess impacts by land cover change. Performance of the SWAT model during calibration and impact assessment for altered periods are measured with Nash-Sutcliffe Efficiency (NSE). Related to the research questions, the following three hypotheses are formulated:

1. Given the research findings in (T. H. M. Rientjes et al., 2011a) on land cover change in the Gilgel Abay catchment, for this study, it is hypothesized that agricultural area increases.
2. Comparing water balance components of altered period 4 with that of the baseline period, the actual evapotranspiration is expected to increase as the forest cover increase.
3. The hydrologic components of the catchment are highly affected by the changes in land cover.

In the current study, the gradual land cover changes of the study catchment are diagnosed in five periods: baseline period, i.e., 1986 to 1994, and four altered periods, i.e., 1995-2001, 2002-2008, 2009-2013 and 2014-2018. For the altered periods, two scenarios are carried out, i.e. without land cover change (using LC map of only 1986 for the four periods) and with land cover change (using land cover maps of 2001, 2008, 2013 and 2018). The baseline period (1986–1994) served calibration SWAT model using land cover map of 1986. The calibrated model parameter set then is applied for the altered periods to assess deterioration of model performance using the Nash Sutcliffe efficiency (NSE). As in Marhaento et al. (2017), who also applied the SWAT model and who used NSE as an indicator to assess land cover change impacts on runoff hydrology and water balance, it is hypothesised that NSE continuously decreases from baseline to altered periods. The steeper decrease of NSE is expected without land cover change than with LC change (Figure 1). Any deterioration with reference to the baseline period indicates that land cover changes impacted runoff hydrology and water balance of the catchment.

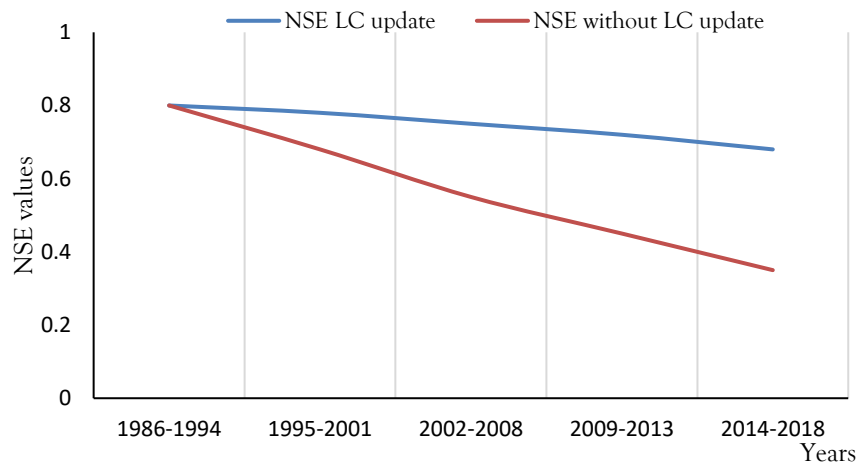


Figure 1: Hypothetical scenarios to test NSE for model simulation with/without LC change adapted from Marhaento et al. (2017)

2. LITERATURE REVIEW

2.1. Land cover change

The term land cover (LC) refers to the type of covers such as forest or grass, but it has broadened in successive usage to include other things such as human structures, soil type, biodiversity, surface and groundwater (Meyer et al., 1995). According to Meyer et al. (1995), every parcel of land on the Earth's surface is unique in the cover it possesses. LC are distinct yet closely linked characteristics of the Earth's surface. The land cover categories could be cropland, forest, wetland, pasture, roads, settlement areas among others.

The main drivers and factors contributing to land cover changes include increasing population and livestock, reduced distances from various infrastructures such as roads and markets/urban areas, and topographic factors such as slope, and land degradation. In the study area, major changes in land cover have been observed in the past two to three decades (Yalew et al., 2018). The land cover changes have generally resulted in the expansion of agricultural lands at the expense of other land covers such as bare land and grasslands. Their LC change analysis show between 1986 and 2009 cultivated area and plantation forest increased by about 15% and 3% in a while both natural woody vegetation and grassland decreased by about 3%. T. H. M. Rientjes et al. (2011a) study show expansion of agricultural area by 1.53%. However, their finding indicated that between the years 1973-1986, forest cover decreased by 1.38%.

2.2. Effects of land cover changes on hydrological processes

Land cover characteristics have many connections with the hydrological cycle. The Land cover types determine the amount of rainwater interception and affect the infiltration capacity of the soil and thus the runoff amount by following the falling of precipitation (Hudson et al., 2002). Land cover directly affects the amount of evaporation, groundwater infiltration and overland runoff that occurs during and after precipitation events. These factors control the water yields of surface streams and groundwater aquifers and thus the amount of water available for both ecosystem function and human use (Fisher and Mustard, 2004)

Land cover change commonly is by human intervention that may affect rainfall-runoff relationships (e.g. Wang et al., 2017). When land cover changes such may result in changes in canopy cover, degradation of the vegetative cover, and increased soil disturbance that increase surface runoff and soil erosion (Ajayi, 2004). For instance, a dense vegetation cover shields the soil from the raindrop impact and reduces the detachment of the soil. As well, it retards the velocity surface flow particularly on gentle slopes, giving the water more time to infiltrate into the soil layer.

Land cover change may impact hydrology, socio-economics, ecological, and the environment (Zheng, 2016). Changes in LC may alter both runoff behaviour and the balance that exists between evaporation, groundwater recharge and streamflow discharge in specific areas and the entire watershed. The impact of land cover changes on hydrology is immediate and long-lasting. In the short term (< 2 years), destructive land cover change may affect the hydrological cycle either through increasing the water yield or diminishing or even eliminating the low flow in some circumstances (T. H. M. Rientjes et al., 2011a). In the long term (> 5 years), the effect of LC change extends to the water sources, both surface and groundwater (Abebe, 2005). Changes in land cover alter both runoff behaviour and the balance that exists between evaporation, groundwater recharge and stream discharge in specific areas and entire watersheds, with considerable consequence for all water sources and users (Eshleman, 2004). Understanding how LC changes impact water

balance components, which is part of the objective in this study, can help to develop a strategic plan to preserve a watershed (Pokhrel, 2018). The current study builds on the previous studies by additionally diagnosing if the changes in LC propagate in modelling.

Dynamic modelling gives leverage to understanding the effect of LC changes on water balance components. The rational way to model the impact of land cover changes on runoff dynamics of a river catchment is through the implementation of spatially distributed physical based hydrological model (Chen et al., 2004). Yalew et al. (2018) applied an integrated modelling approach to assess the interactions of land and water resources of Upper Blue Nile. Yalew et al. (2018) modelling results showed that land cover change influences hydrologic response, demonstrated using streamflow responses. Likewise, hydrologic processes and water resources availability is shown to influence land cover suitability and hence land cover change responses. Relevant to the upper Gilgel Abay catchment, Gumindoga et al. (2014) studied the effect of land cover change on predicting streamflow using remote sensing satellite data and based on the TOPMODEL approach. Results showed that the highest peak flow and the annual streamflow volume varied among the land cover types, that includes agriculture, forest and grassland which dominate land cover in the catchment. Results of this study show that in scarce data satellite images provide suitable land surface data for rainfall-runoff modelling and land surface parameterisation. T. H. M. Rientjes et al. (2011a) applied HBV model, GIS and satellite images to assess the hydrological response of land cover in Gilgel Abay catchment. The study shows a peak flow increase and a base flow decrease by $0.762 \text{ m}^3/\text{s}$ and $0.069 \text{ m}^3/\text{s}$ respectively. Generally, the analysis indicated that the flow during the wet season has increased, while it decreased during the dry period.

2.3. Hydrological model

Hydrologic models are simplified conceptual representations of reality, in this case, part of the hydrologic, or water cycle. The models are primarily used for hydrologic prediction and for understanding hydrologic processes. The catchment hydrologic models have been developed for many different reasons and therefore have many different forms (Gayathri et al., 2015). However, they are in general designed to meet one of the two primary objectives. One objective of catchment modelling is to gain a better understanding of the hydrologic phenomena operating in a catchment and of how changes in the catchment may affect these phenomena. Another objective of catchment modelling is the generation of synthetic sequences of hydrologic data for facility design or use in forecasting. They also provide valuable information for studying the potential impacts of changes in land cover.

Hydrological models are classified based on model input and parameters and the extent of physical principles applied in the model. Considering model parameters as a function of space and time, a hydrological model can be classified as a lumped and distributed. In a lumped model, the entire river basin is taken as a single unit, and the model outputs do not consider the spatial processes whereas a distributed model can make predictions that are distributed in space so that the parameters, inputs and outputs can vary spatially (Devia and Ganasri, 2015). Models can also be classified as deterministic and stochastic models based. (T. Rientjes 2015). Another classification is static and dynamic models whereby static model excludes time while the dynamic model includes time (Devia and Ganasri, 2015). According to (Devia and Ganasri, 2015).one of the most important classifications is an empirical model, conceptual models and physically based models. Empirical models are observation-oriented models which take only the information from the existing data without considering the processes of the hydrological system. The empirical model involves mathematical equations derived from concurrent input and output time series and not from the physical processes of the catchment.

Conceptual models consist of a number of interconnected reservoirs which represents the physical elements in a catchment. In this method, semi-empirical equations are used to describe the physical elements.

Physically based model uses a mathematical representation to express the real phenomenon in the catchment. It uses state variables which are measurable and are functions of both time and space. The hydrological processes of water movement are represented by finite difference equations.

Table 1: Types of hydrological models adapted from (Tegegne et al. 2017)

Empirical model	Conceptual model	Physically based model
Data based or metric or black box model	Parametric or grey box model	Mechanic or white box model
Involve mathematical equations, derive values from available time series	Based on modelling of reservoirs and include semi-empirical equations with a physical basis	Based on spatial distribution, evaluation of parameters describing physical characteristics
Little consideration of features and process system	Parameters are derived from field data and calibration	Require data about the initial state of model and morphology of catchment
High predictive power, low explanatory depth	Simple and can easily be implemented in computer code	Complex model. Require human expertise and computation capability
Cannot generate to other catchments	Require large hydrological and meteorological data	Suffer from scale related problems
ANN, unit hydrograph	HBV model, TOPMODEL	SHE or MIKESHE model, SWAT
Valid within the boundary of a given domain	Calibration involves curve fitting make difficult physical interpretation	Valid for a wide range of situations

2.3.1. Criteria for model selection

Many criteria can be used for choosing the “right” hydrologic model. In most situations, simple objective methods of selecting the best model for a particular study was developed by (Marshall et al., 2005), so those criteria can be used to choose between alternative models:

1. Accuracy of prediction
2. The simplicity of the model
3. The consistency of parameter estimates
4. The sensitivity of the results to changes in parameter values.

The development of Geographic Information Systems (GIS) and remote sensing techniques, the hydrological models have been more physically based and distributed to enumerate various interactive hydrological processes considering spatial heterogeneity. Hence, the ability of a hydrological model to integrate GIS for hydrologic data development, spatial model layers and interface may be considered as model selection criteria. For the accomplishment of objectives of the current study, the effect of land cover changes on the water balance components of Gilgel Abay watershed, the following model selection criteria will be considered:

- applicability over a range of catchment sizes
- capability to consider land cover change effect
- the model has been used for water-balance studies
- ability to predict the impact of management practices on streamflow
- the model able to use data from various global databases
- the model is readily and freely available with good documentation

For this study, depending on the above criteria SWAT is selected as an appropriate model to meet the simulation requirements set above using available soil, topography, land cover and weather data.

2.3.2. SWAT model

The SWAT model is a semi-distributed, time-continuous watershed simulator operating on a daily time step (Arnold et al., 2012a). The inputs of SWAT data are DEM, land cover map, soil data, climatic data and streamflow data. The semi-distributed model domains are based on Hydrological Response Unites (HRU's) that result from overlaying maps for soils, slopes and lands cover. For each unique combination of soil, slope and landcover HRU is defined. The principle to HRU is that all HRU's that belong to each specific combination of soil, slope and land cover is assumed to have exact similar hydrological behaviour. During model calibration, each defined HRU has unique model parameter set. Such an approach allows application in ungauged catchment areas in case HRU's in gauged basin area also are present in ungauged parts of a catchment area. The latter applies to the Gilgel Abay area with about 45% of are that that is gauged (i.e. the Upper Gilgel Abay) and the remaining part that is ungauged (see Figure 6). The SWAT model simulates the water balance of the catchment and give outputs such as surface runoff, evapotranspiration, groundwater discharge, lateral discharge and actual evapotranspiration. (See Appendix)

2.3.3. Simulation of the hydrological components using the SWAT model

The Simulation of the hydrology of a watershed is done in two separate steps (Marhaento et al., 2017). Step one is the land phase of the hydrological cycle that assess the amount of water, sediment, nutrient and pesticide to the main channel in each sub-basin. Hydrological components simulated in land phase of the Hydrological cycle are canopy storage, infiltration, redistribution, evapotranspiration, lateral subsurface flow, surface runoff, ponds, tributary channels and return flow (Neitsch et al., 2004). The second step is the routing phase that can be defined as the movement of water, sediments, nutrients and organic chemicals through the channel network of the watershed to the outlet. In the land phase of the hydrological cycle, SWAT simulates the hydrological cycle based on the following water balance equation.

$$SW_t = SW_o + \sum_{i=1}^t (R_{day} + Q_{surf} - E_a - W_{seep} - Q_{gw}) \quad 1$$

Where SW_t is the final soil water content at the end of t days (mm), SW_o is the initial soil water content (mm), t is the time (days), R_{day} is the amount of precipitation on day i (mm), Q_{surf} is the amount of surface runoff on day i (mm), E_a is the amount of evapotranspiration on day i (mm), W_{seep} is the amount of water entering the vadose zone from the soil profile on day i (mm), and Q_{gw} is the amount of return flow on day i (mm). More detailed descriptions of the different model components are listed in (Neitsch, 2005).

In the SWAT model, Manning's equation is used to define the rate and velocity of flow. The channel cross-section and longitudinal slope are computed from the digital elevation model (DEM). Once the model determines flow to the main channel, it is routed through the stream network using a command structure

similar to that of HYMO (a problem-oriented computer language for building hydrologic models). (Williams and Hann, 1972) and (Arnold et al., 2012a) developed the Routing Outputs to Outlet (ROTO) model that later merged to SWAT2005 to route the flows through channels and reservoirs to support an assessment of the downstream impact of water management. Flow routing is done through the channel using a variable storage coefficient method developed by the Muskingum routing method (Williams and Hann, 1972).

2.3.4. Model calibration

Calibration is the optimization of parameter values and comparison of the predicted output of interest to measured data until a defined objective function is achieved (Neitsch, 2005). Parameters for optimization are selected from those identified by the sensitivity analysis (Arnold et al. 2012). Additional parameters, other than those identified during sensitivity analysis, are used primarily for calibration due to the hydrological processes naturally occurring in the watershed. Sometimes it is necessary to change parameters in the calibration process other than those identified during sensitivity analysis because of the type of miss match of the observed variables and the predicted variables (White and Chaubey, 2005).

According to S, Neitsch et al, (2004), the values GWQ (Groundwater discharge) and SURQ (Surface runoff) in the SWAT output files cannot be used directly because in-stream precipitation, evaporation, transmission losses, etc. will alter the net water yield from that predicted by the WYLD (Water yield) variable. Groundwater and surface runoff are therefore calibrated by assuming that the effect of in-stream precipitation, evaporation and other losses from the river do not have significant influence.

The performance of model simulation should also be tested against an independent set of observed data (Moriassi et al. 2007) . This procedure helps to demonstrate the predictive capability of the model.

2.3.5. Model performance analysis

In regarding evaluating the accuracy of the overall model calibration and validation, statistical indicators like Nash-Sutcliffe efficiency (NSE) are used Nash-Sutcliffe Efficiency (NSE) is defined as the difference between the simulated and observed values which is normalized by the variance of the observed value (Nash & Sutcliffe 1970). NSE is selected in this study for the reason that it has better accuracy than the other objective function (Krause et al., 2005). NSE is calculated using the following equation:

$$NSE = 1 - \frac{\sum_{i=1}^n (S_i - O_i)^2}{\sum_{i=1}^n (\bar{O} - O_i)^2} \quad 2$$

where S_i = model simulated output; O_i = observed hydrologic variable; \bar{O} = mean of the observed. The NSE= Nash-Sutcliffe efficiency and n is the total number of observations.

The Nash-Sutcliffe simulation efficiency (NSE) indicates how good the observed versus simulated value fits on the 1:1 line plot. If the measured value is the same as all predictions, NSE is 1. If the NSE is between 0 and 1, it indicates deviations between measured and predicted values. If NSE is negative, predictions are very poor, and the average value of output is a better estimate than the model prediction (Nash and Sutcliffe, 1970). The evaluation of the model accuracy has been based on performance ratings: very good, good, satisfactory and unsatisfactory. Table 2 presents model performance evaluation criteria as suggested by (Moriassi et al., 2007)

Table 2: Model performance rating criteria, source from (Moriassi et al., 2007)

Rate	NSE
Very good	$0.75 < \text{NSE} \leq 1$
GOOD	$0.65 < \text{NSE} \leq 0.75$
Satisfactory	$0.5 < \text{NSE} \leq 0.65$
Unsatisfactory	$\text{NSE} \leq 0.5$

3. MATERIALS AND METHODS

3.1. Study area and data

3.1.1. Study area

Gilgel Abay catchment is located in the Northwest part of Ethiopia between 10°56' to 11°51' N latitude and 36°44' to 37°23'E longitudes. The Gilgel Abay river flows between Gish Abay spring located at the mountainous south of the basin and the outlet lake that is south of Lake Tana. Gilgel Abay river is the largest tributary of the Lake Tana basin (Uhlenbrook et al., 2010). This study applied two catchment levels. The first is the upper Gilgel Abay catchment considering Wetet Abay as the gauging station. The second is the Gilgel Abay catchment considering the river outlet section where Gilgel Abay joins Lake Tana. Owing to the gauging station and thus observed data at Wetet Abay, the performance of the SWAT model was evaluated by calibrating and simulating the model for the upper Gilgel Abay catchment. Detection of land cover change and the effect of land cover changes on water balance components were assessed for the whole Gilgel Abay catchment at the outlet to Lake Tana. The calibrated model parameters using the upper Gilgel Abay catchment were transferred for the model simulation at the whole catchment level.

Figure 2 shows Gilgel Abay catchment (3752 km²) at the Gilgel Abay river outlet to Lake Tana. The elevation ranges from 3510 m to 1787 m.a.s.l. The catchment has a rough landscape and plateau with gentle slopes. The geology of the area is composed of quaternary basalts and alluviums. The soil is mostly covered by clays and clayey loams. The largest land cover unit is an agricultural area. The rainfall of Gilgel Abay that originates from moist air coming from the Atlantic and Indian oceans follows the north-south movement of the Inter-Tropical Convergence Zone (Mohamed et al., 2005). The Ethiopian climate is mainly influenced by the intertropical convergence zone (ICTZ) and topography of the area on the local climate. Table 3 shows a traditional climate classification in the country (NMSA, 2001). The largest part of this study area falls in Woina-Dega climate. The upstream part of the catchment falls in Dega Zone. There is a high spatial and temporal variation of rainfall in the study area.

Table 3: Climate classification in Ethiopia (source: (NMSA, 2001).

Climatic zones	Elevation	Description
Wurch	>3000 m	cold climate
Dega	3000-2500 m	temperate like climate-highland
Woina-Dega	2500-1500 m	Warm climate
Kola	<1500 m	hot and hyper-arid type

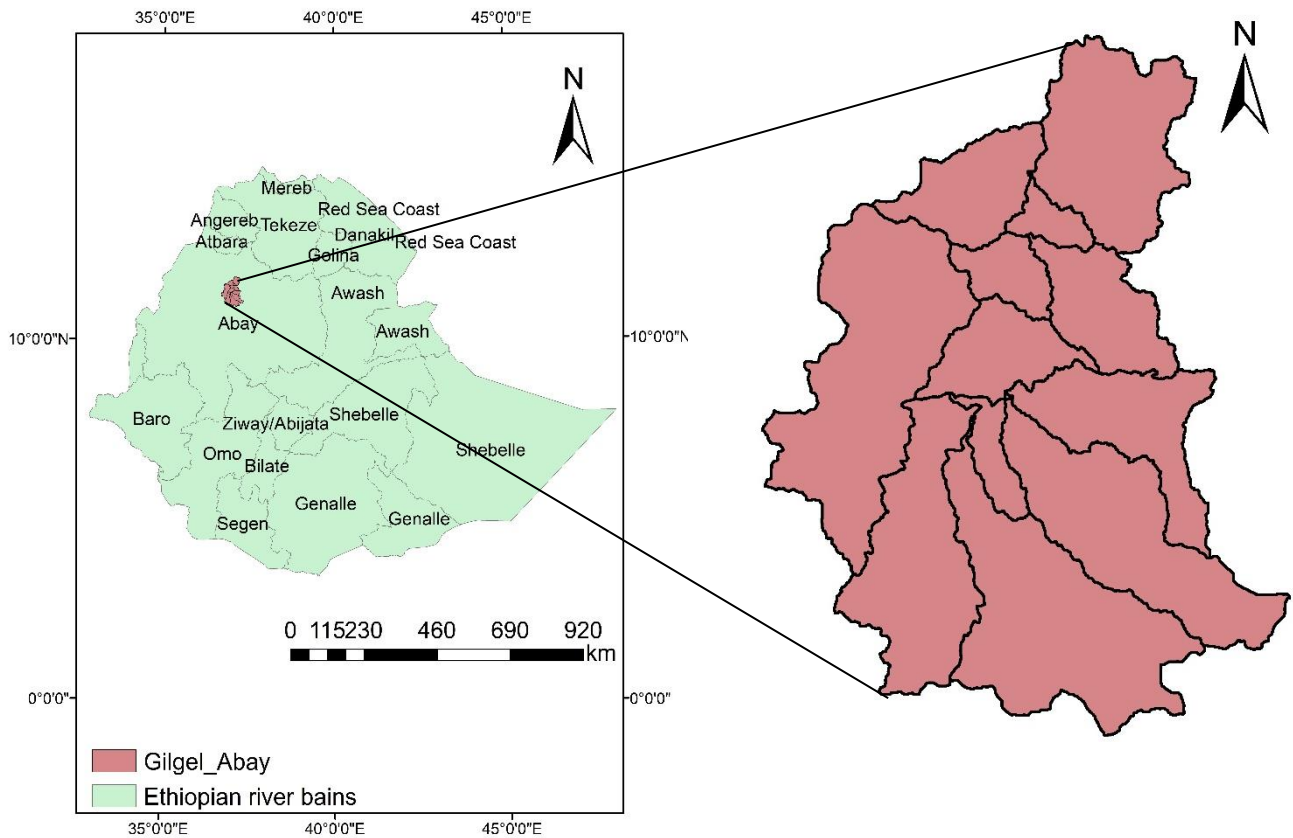


Figure 2: The study area

3.1.2. Data

This study involves the use of a semi-distributed hydrological model that requires extensive hydrometeorological and spatial data that include:

- Spatial data: soil types, land cover and topographic data
- Hydrological data: streamflow
- Meteorological data: precipitation, temperature, relative humidity, sunshine hour and wind speed.

I) Soil data

The soil data include soil texture, available water content, hydraulic conductivity, bulk density and organic carbon content for a different layer and soil types. The soil data having 250m resolution was collected from the Ministry of Agriculture and Natural Resource of Ethiopia. The soil map of Gilgel Abay catchment has seven soil classes as shown in Figure 3.

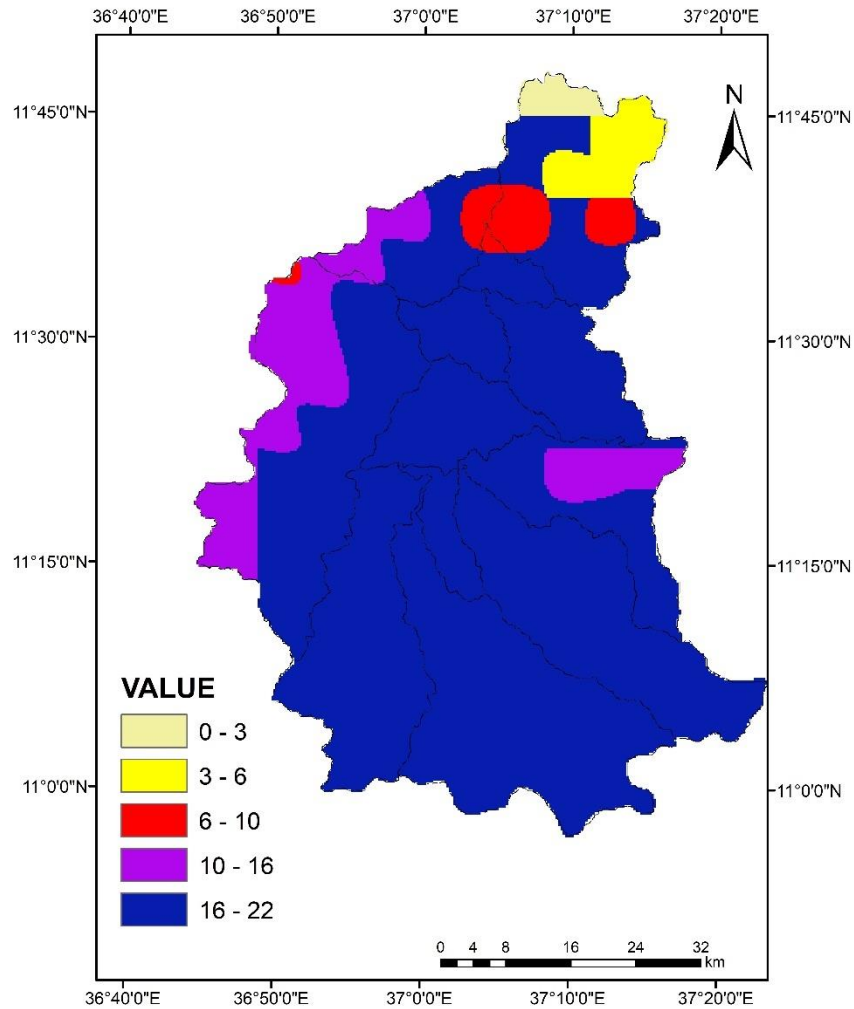


Figure 3: Soil map of the study area

II) DEM data

The slopes, elevation and stream networks of the Gilgel Abay catchment were extracted from the digital elevation model (DEM) data. The DEM data with 30 m resolution was downloaded from Shuttle Radar Topography Mission (SRTM) from <https://earthexplorer.usgs.gov/>. The elevation of Gilgel Abay catchment ranges from 1787 to 3510 m.a.s.l. The DEM data of the Gilgel Abay catchment is shown in Figure 4.

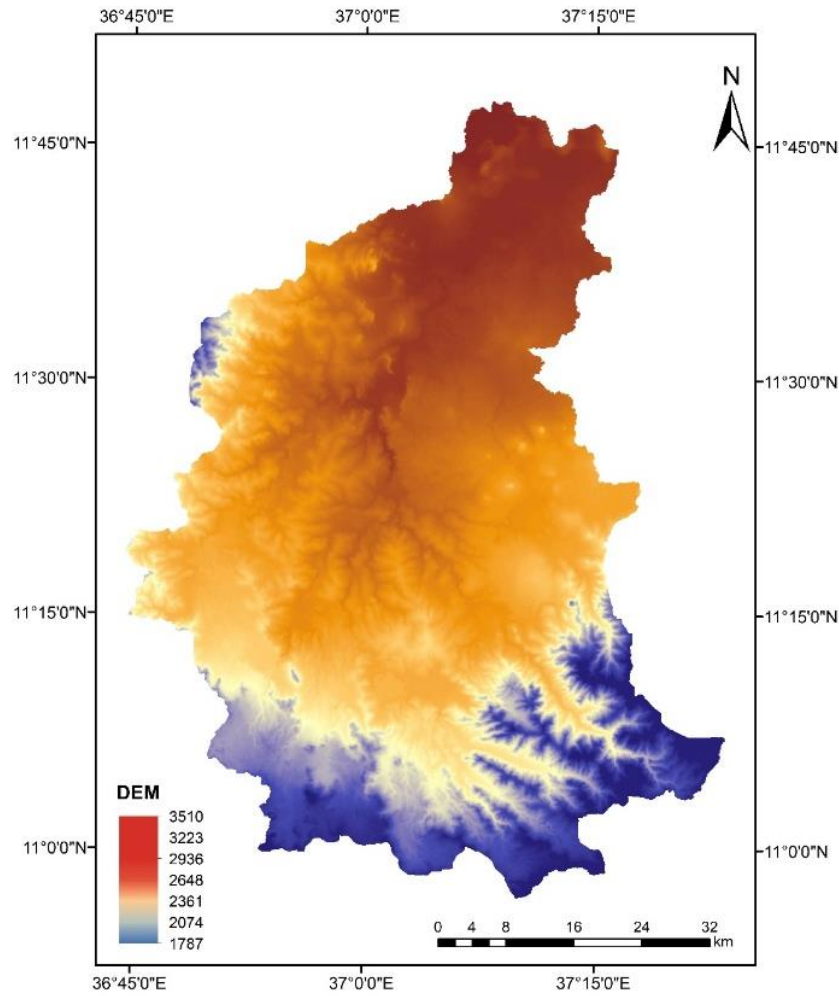


Figure 4: DEM of Gilgel Abay catchment

III) Land cover data

Land cover is one of the most important inputs of the hydrological model. The satellite imagery for the years 1986, 2001, 2008, 2013 and 2018 was used to generate the land cover map. The satellite imagery of Landsat Thematic Mapper (TM) of 1986, 2001 and 2018 at a spatial resolution of 30m were downloaded from USGS Earth Explorer (<https://earthexplorer.usgs.gov/>). Land cover map of 2008 and 2013 at a spatial resolution of 30m, which were collected having from Ethiopian mapping agency (EMA), were merged from thirteen to six land cover types. The type of sensor, date of acquisition and the source of the Landsat images/ land cover maps for 1986, 2001, 2008, 2013 and 2018 are described in Table 4.

Table 4: Description of Landsat images

Year	Sensor	Date acquisition	Resolution	Source of data
1986	Land sat 5 TM	12/01/1986	30m	https://earthexplorer.usgs.gov/
2001	Land sat 5 TM	20/01/2008	30m	
2008	Land sat 7	January 2008	30m	Ethiopian mapping agency
2013	Land sat 7	January 2013	30m	
2018	Land sat 8 OLI	28/01/2018	30m	https://earthexplorer.usgs.gov/

Ground control points (GCPs)

In the classification of land cover using satellite images and GIS-based techniques, ground control points (GCPs) serve to determine the relationship between remotely sensed data and the object (i.e. specific land cover on the ground). In this study GCPs were collected from two sources: 150 GCPs from the field survey using GPS and 330 GCPs from google earth. The GCPs that were collected from the field survey were exported to google earth and showed similar land cover type. The GCPs were collected by applying a stratified and random sampling method as suggested in (Congalton, 1990). These GCPs were used to produce signature for supervised classification and accuracy assessment of satellite images of the watershed. The GCPs from the two sources were combined using the tool of intersection on ArcGIS for respective representative LC types. Those combined LC types were 146 points for Agricultural land, 29 points for residential, 179 points for Forest, 39 points for Grassland, 60 points for Bare Soils, 7 points for shrub and bushland and 14 points for Water and wetland.

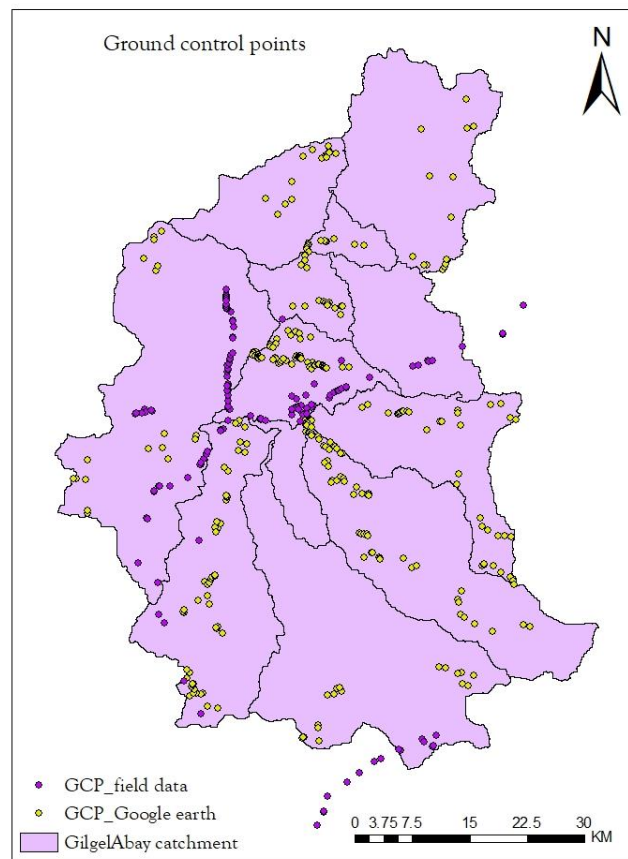


Figure 5: Ground control points (GCP) from google earth and from field data

IV) Hydro metrological data

Streamflow data

Daily flow data of twenty-one years of Gilgel Abay catchment at Wetet Abay monitoring station was collected from MOWIE. The SWAT model was calibrated at Wetet Abay gauging station (see Figure 6). The observed data at Wetet Abay gauging station is from 1986 to 2008, which is enough only for the three windows, i.e., baseline (BL), altered period 1 (AP1) from 1995-2001 and altered period 2 (AP2) from 2002-2008. The absence of observed data for AP3 and AP4, i.e., from 2009-2013 and 2014-2016 were overcome by simulating with SWAT. After calibrating AP2 using data of the closest window (AP2), the parameter set

were transferred to simulate discharge for AP3 and AP4. Simulated discharge of AP3 and AP4 were assumed to represent the observed data.

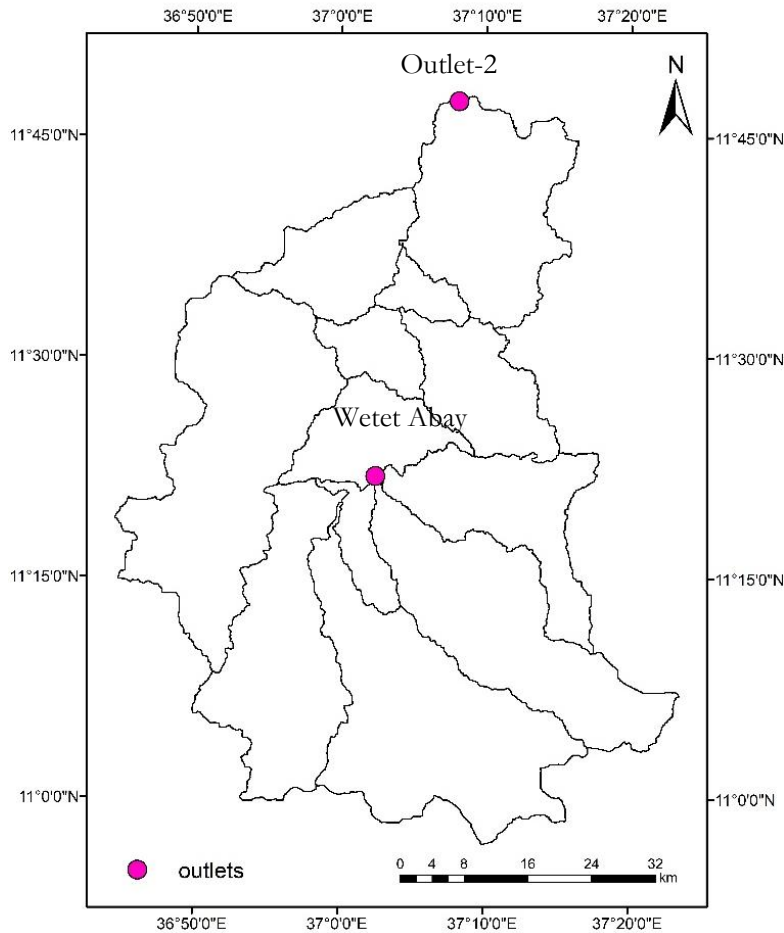


Figure 6: Gauged station (Wetet Abay) and ungauged outlet.

The above map shows the outlets of the catchment Wetet Abay gauged station and outlet-2 is the outlet to the Lake Tana and it is not Gauged.

Meteorological data

Daily data recorded at eight meteorological stations Adet, BahirDar airport, Chambal, Dangla, Enjibara, Kidamaja, Sekela and Wetet Abay were collected from National Meteorological Service Agency (NMSA). Those daily data are precipitation (presented in Appendix), maximum temperature, minimum temperature and weather information like wind speed, sunshine hours and relative humidity. The available meteorological data are from 1986-2016. Table 5 presents the coordinate, elevation and mean annual rainfall of the eight stations considered in the study area.

Table 5: Coordinates and elevation of the metrological stations in Gilgal Abay catchment

Meteorological stations	Locations			Mean annual Rainfall (mm)
	Longitude (°)	Latitude (°)	Elevation (m)	
Adet	37.49312	11.2745	2080	1168.866
BahirDar Airport	37.322	11.6027	1829	1321.907
Chimba	36.846	11.4337	2143	1392.493
Dangla	36.9193	10.9954	2670	1601.852
Enjibara	36.679	10.9989	2450	2203.562
Kidamaja	37.204	10.97	2690	1723.693
Sekela	37.04228	11.37	1913	1947.288
Wetet Abay	37.00	11.603	2806	1545.14

Figure 7 shows the mean annual rainfall (1986-2016) of stations in the study area. The mean annual rainfall ranges from around 1200 to 2400 mm. Enjibara has the highest mean annual rainfall of all stations in the catchment and Adet has the lowest mean annual rainfall.

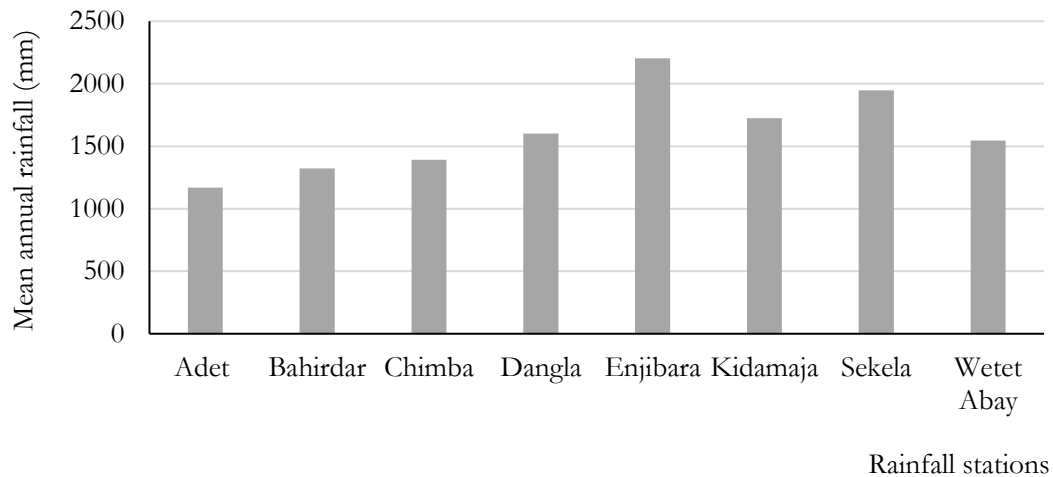


Figure 7: Mean annual rainfall of meteorological stations in Gilgal Abay catchment.

Figure 8 shows the relationship between elevation and mean annual rainfall of the eight meteorological stations in the Gilgal Abay catchment. In general, the mean annual rainfall increases as elevation increases.

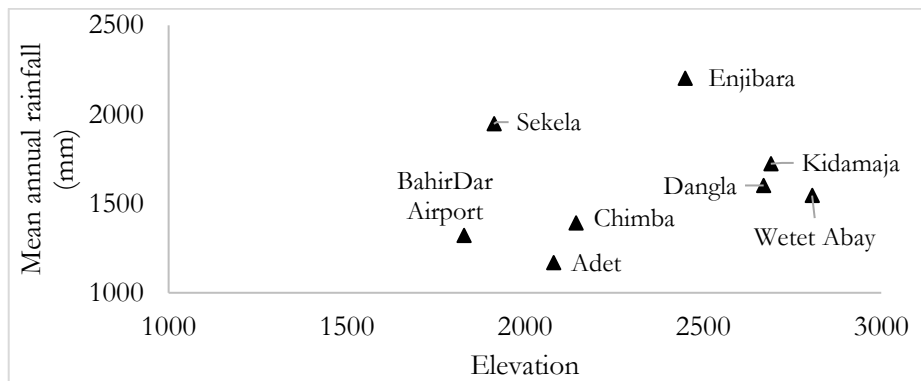


Figure 8: Relationship of elevation versus mean annual rainfall of the meteorological stations in Gilgal Abay catchment.

Figure 9 shows eight meteorological stations spatially distributed in Gilgel Abay catchment. The stations are not evenly distributed in the catchment.

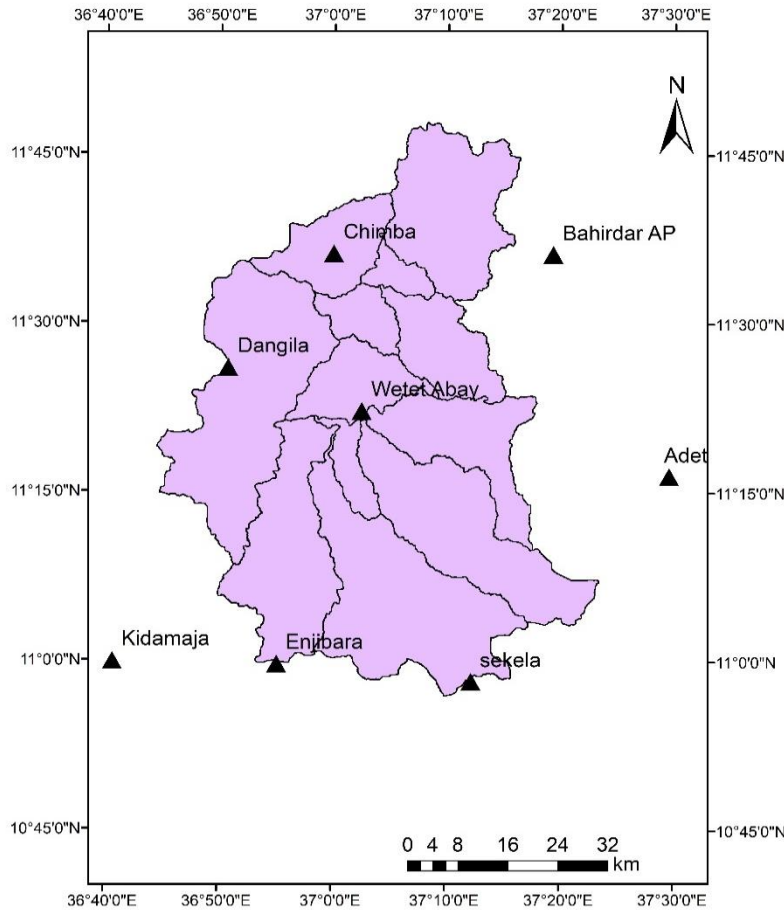


Figure 9: Map of weather stations in the catchment

3.2. Methods

In the current study, the effect of land cover change will be evaluated on water balance components such as streamflow and actual evapotranspiration between 1986 and 2018 using the SWAT model. The hydrological simulations will be carried out for two scenarios, with and without land cover updates, adapted from the approach in Marhaento (2018). The SWAT simulation was divided into five windows to diagnose gradual land cover changes in the catchment. The first period (1986–1994) was regarded as the baseline period (BL) and the periods (1995–2001, 2002–2008 and 2009–2013, 2014–2018) were regarded as altered periods. The five land cover maps produced for the years 1986, 2001, 2008, 2013 and 2018 represent the land cover status for each period. The baseline period (1986–1994) was used for calibrating SWAT model using land cover map of 1986 and then was applied for the altered periods.

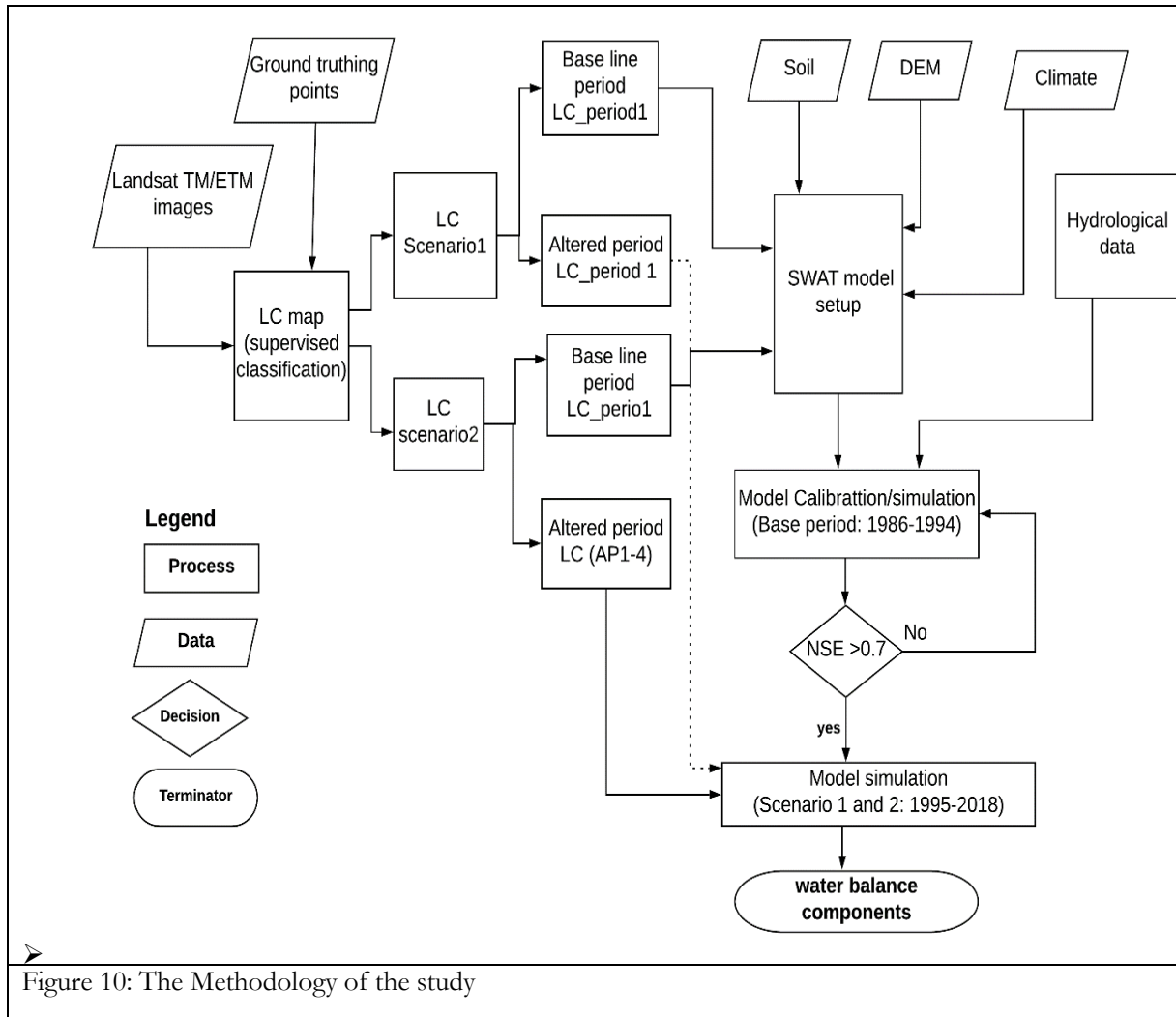


Figure 10: The Methodology of the study

shows the step by step procedure of the method applied in the study.

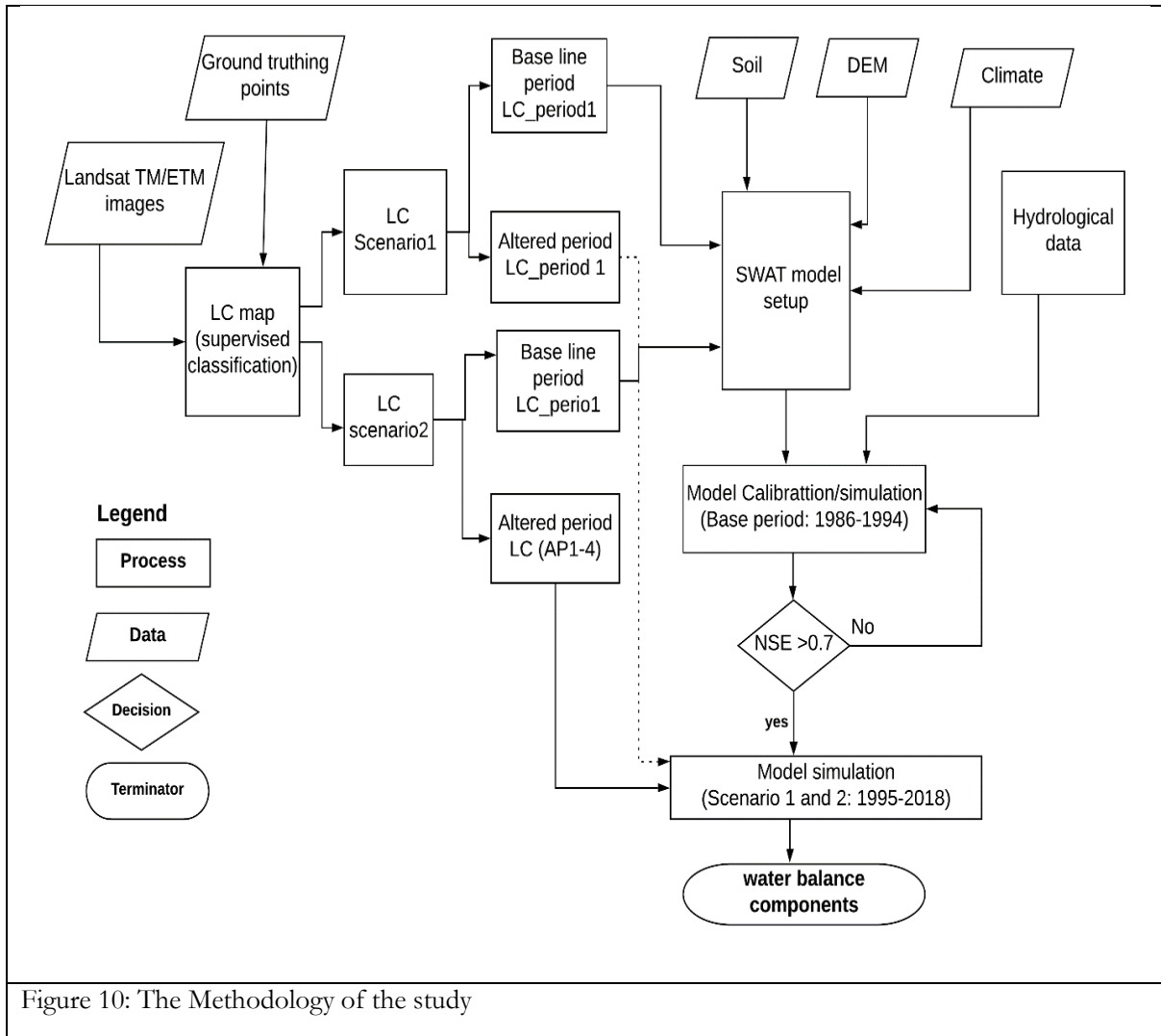


Figure 10: The Methodology of the study

3.2.1. Image processing and classification

Image processing

Landsat satellite images were used to identify changes in land cover distribution in Gilgel Abay catchment from 1986 to 2018. For this Windows, five images were selected to produce land cover maps. For each image processing was performed that includes layer stacking and subsetting. Figure 11 describes the procedure of producing the LC map.

Layer Stacking images - In order to analyze remotely sensed images, the different images representing different bands must be stacked. This allows different combinations of RGB to be shown in the view. Therefore, the layer stack is often used to combine separate image bands into a single multispectral image file. **Subsetting**, the process of “cropping” or cutting out a portion of an image for further processing an image, can be useful when working with large images. Subsetting of Gilgel Abay catchment satellite image was performed using the layer stacked image by the delineated watershed shapefile.

Image classification

The purpose of the image classification process is to categorize all pixels in a digital image into one of several land cover classes, or "themes". This classified data may then be used to produce thematic maps of the land cover. Normally, multispectral data are used to perform the classification. The spectral pattern present within the data for each pixel is used as the numerical basis for categorization (Lillesand et al., 2014). The aim of image classification is to identify and portray, as a unique grey level (or colour), the features occurring in an image in terms of the object or type of land cover these features represent on the ground. The two

main image classification methods are supervised and unsupervised Classification. In this study supervised classification is applied as it has better accuracy. Image classification was performed using Arc GIS.

Supervised classification

With supervised classification, it can be identifying examples of the Information classes (i.e., land cover type) of interest in the image. These are signature files from GCPs. The statistical characterization of the reflectance for each information class was developed using the image processing software system. Once a statistical characterization has been achieved for each information class, the image is classified by examining the reflectance for each pixel and making a decision about which of the signatures it resembles most. (Eastman, 2001) creates a signature file from the training samples, which is then used by the multivariate classification tools to classify the image. Typically, a maximum likelihood of descriptor is used to measure the spread of values around the mean of the class. Each pixel of the image is assigned as far as possible to one of the land cover groups, as defined by the signature.

Merging of land cover maps

For this study, six representative LC types were selected in order not get complicated SWAT model. Those are forest, agricultural land, bare land, grassland, residential and wetland. Although the maps from Ethiopian mapping agency (EMA) of 2008 and 2013 was done with supervised classification they had 13 and 17 land cover respectively. The merging mechanism is done by using ArcGIS. The following flow chart shows the procedure of merging. The land cover types of 2008 as shown in Land coverage, interception and infiltration capacity were some of the criteria used as the criterion for merging.

Table 6. dense forest, moderate forest, sparse forest into forest, open grassland, open shrubland and bare land merged into bare land, closed grassland into grassland, annual cropland into agricultural land, residential land into agricultural land, water into a wetland. LC 2013 also as listed in Land coverage, interception and infiltration capacity were some of the criteria used as the criterion for merging.

Table 6 shows dense forest, sparse forest, woodland merged into forest, open shrubland, Bare land, Lava flow, Salt span into bare land, closed grassland and closed shrubland merged into grassland, perennial crop, annual crop merged into agricultural land, Wetland and Water into wetland and residential in to residential. Land coverage, interception and infiltration capacity were some of the criteria used as the criterion for merging.

Table 6: Merging of land cover maps 2008 and 2013

2008 LC map	2013 LC map	Merged LC types
Dense forest Moderate forest Sparse forest	Dense forest Sparse forest Woodland	Forest
Open grassland Open shrubland Bare land	Bare land Lava flow Salt span Open shrubland	Bare land
Closed grassland	Closed grassland Closed shrubland	Grassland
Residential	Residential	Residential
Annual crop	Perennial crop Annual crop	Agricultural
Water	Wetland Water	Wetland

Steps of classifying Land cover

Step 1. *Collecting of training*: By Collecting of training samples to sort classes and compute their signatures. Training samples can be created collectively using the drawing tools training samples on the image classification toolbar. If the bands' number in the image is n , the best amount of pixels for each training sample was between $10n$ and $100n$.

Step 2. *Evaluating training samples*: Since the training samples are drawn in the display, new classes are generated automatically in the TSM. This manager provides three tools for evaluating the training samples. Those are the *histograms tool*, the *Scatterplots tool*, and the *Statistics tool*. Those tools used to explore the spectral features of different areas. Additional tools used to assess training samples to see if there is enough separation between the classes.

Step 3. *Editing classes*: According to the result of the evaluation of the training sample, the overlapping classes should be merged into one class by using the *Merge tool*. Finally, the Class name, the display colour, save and load training samples should be finished.

Step 4. *Creating the signature file*: The determined training samples are representative of the selected classes and are unique from one another, a signature file generated using the *Create Signature File tool*.

Step 5. *Examining the signature file*: To review the attribute separation between sequentially merged classes in a signature file it has been used the *dendrogram tool* The output is an ASCII file with a tree diagram shows the separation of the classes. The dendrogram used to determine if two or more classes or clusters are unique enough.

Step 6. *Applying classification*: After generating signature file the last step is classification the image. The image is classified by using the Maximum Likelihood Classification tool, the tool based on the maximum likelihood probability theory. In Maximum Likelihood, Classification assigns each pixel to one of the different classes based on the means and variances of signatures class (stored in a signature file).

The procedure of LC maps classification was executed using the following procedure in Figure 11. For the years 1986, 2001 and 2018 Landsat images were downloaded from USGS Earth Explorer. Layer stalking of different bands for producing a multispectral image using ArcGIS. By using multispectral image creating signature files and finally, maximum likelihood supervised classification performed. Validation was done using the GCPs while the maps from EMA was merged and validated with GCPs.

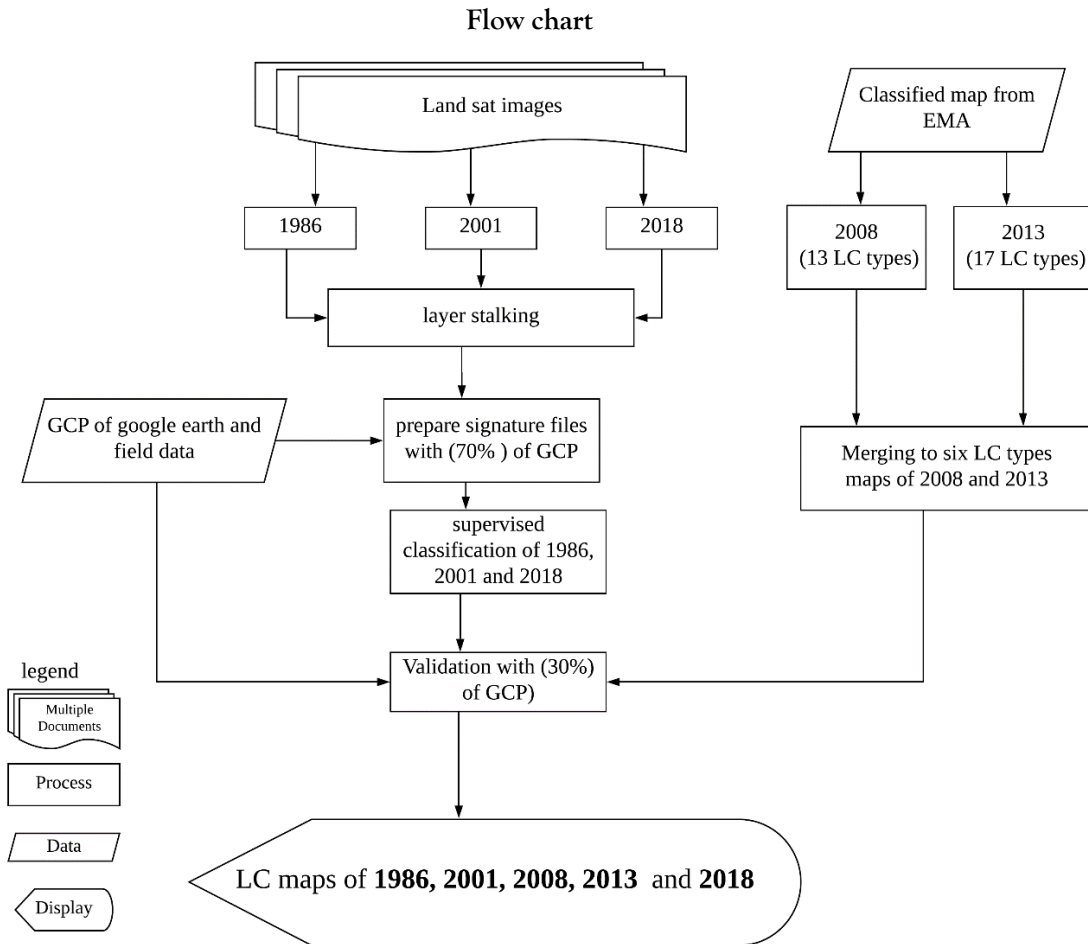


Figure 11: Flowchart showing steps on how to produce the Land cover map

Error analysis of the classification

A confusion matrix lists the values for known cover types of the reference data in the columns and the classified data in the rows. The main diagonal of the matrix lists the correctly classified pixels. Some confusion exists concerning the layout of the matrix. Accuracy assessment is an essential step in the process of analysing remote sensing data. The accuracy assessment is used to determine the degree of ‘correctness’ of a map or classified image.

Overall accuracy is one of the basic accuracy measure. It is calculated by dividing the correctly classified pixels (sum of the values in the main diagonal) by the total number of pixels checked. Besides the overall accuracy, classification accuracy of individual classes can be calculated in a similar manner. Two approaches are possible:

- user’s accuracy, and
- producer’s accuracy.

The **producer’s accuracy** is derived by dividing the number of correct pixels in one class divided by the total number of pixels as derived from the reference data column total. The producer’s accuracy measures how well a certain area has been classified. It includes the error of omission which refers to the proportion of observed features on the ground that are not classified in the map. The more errors of omission exist, the lower the producer’s accuracy.

$$\text{producer's accuracy (\%)} = 100\% - \text{error of omission (\%)}$$

If the correct classified pixels in a class are divided by the total number of pixels that were classified in that class, this measure is called the user's accuracy. The user's accuracy is, therefore, a measure of the reliability of the map. It informs the user how well the map represents what is really on the ground.

One class in the map can have two types of classes on the ground. The 'right' class, which refers to the same land-cover-class in the map and on the ground, and 'wrong' classes, which show a different land-cover on the ground than predicted on the map. The latter classes are referred to as errors of commission. The more errors of commission exist, the lower the user's accuracy.

$$\text{User's accuracy (\%)} = 100(\%) - \text{error of commission (\%)}$$

Kappa Coefficient

The Kappa coefficient is a measure of overall agreement of a matrix. In contrast to the overall accuracy, the ratio of the sum of diagonal values to the total number of cells counts in the matrix. The Kappa coefficient takes also non-diagonal elements into account (Rosenfield and Fitzpatrick-Lins, 1986).

$$K = \frac{N \sum_{i=1}^r X_{ii} - \sum_{i=1}^r (X_{i+} + X_{+i})}{N^2 - \sum_{i=1}^r (X_{i+} + X_{+i})} \quad 3$$

Where, r = number of rows and columns in error matrix, N = total number of observations, X_{ii} = observation in row i and column i, X_{i+} = marginal total of row i, and X_{+i} = marginal total of column i.

Table 7: Shows the range of kappa coefficient and their interpretation adapted from Landis and Koch (1977)

Kapa	Interpretation
< 0	Poor arrangement
0.0-0.20	Slight agreement
0.21-0.40	Fair agreement
0.41-0.60	Moderate agreement
0.61-0.80	Substantial agreement
0.81-1.0	Almost perfect agreement

3.2.2. SWAT model setup

Based on SWAT model watershed delineation, at the outlet of Gilgel Abay catchment or at the entrance of Lake Tana having a watershed area of 3752 km². Overlaying land cover, soil and slope were performed to generate HRUs. Daily climatic data from 1986 - 2016 were inputs during SWAT model simulation. The calibration and simulation carried out from 1986- 1994 and 1995- 2016 respectively on daily basis of stream flow and actual evapotranspiration at Wetet Abay monitoring station using manual calibration with Sequential Uncertainty Fitting (SUFI-2) in SWAT- CUP. The result from the sensitivity analysis of the SWAT model showed that the flow is most sensitive to the soil service conservation (SCS) Curve Number II, the parameter which is related to runoff as a function of soil's permeability, land cover and antecedent soil water conditions (CN2), followed by GW_REVAP which is the groundwater determinant parameter. The other sensitive parameter is OV_N which is Manning's n value for an overland flow of the watershed and the soil properties of the watershed are SOL_Z, ESCO and SOL_AWC. LC also shows that the surface runoff significantly increases from July to August and decreases from August to September. It can be concluded that the spatial and temporal distribution of LC class contributes to the change of surface runoff amount in the catchment.

Figure 12. SWAT model including detailed theoretical background on the model's components, descriptions of hydrological processes and Input/output file documentation are found in (Neitsch, 2005).

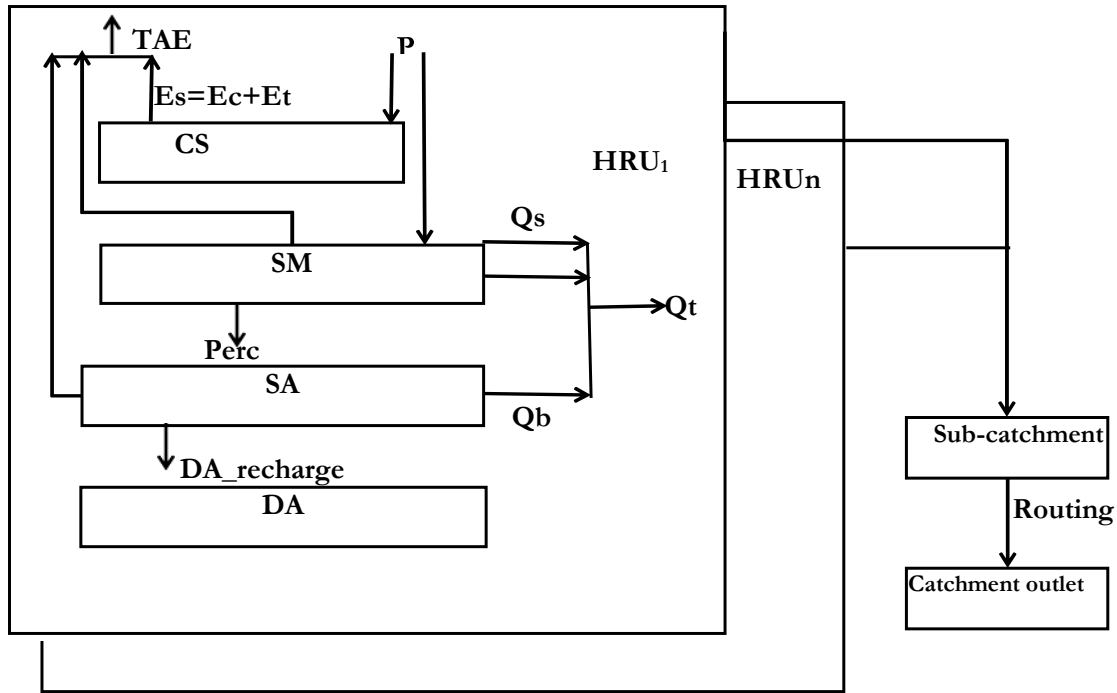


Figure 12: SWAT model structure representation adapted from (Mekonnen et al., 2018)

P is precipitation; CS is canopy storage; TAE is total actual evapotranspiration; E_c is evaporation from the canopy surface; E_s is evaporation from the soil surface; E_t is transpiration from plants; Perc is percolation from the soil storage to shallow aquifer; SM is soil-moisture storage; SA is shallow aquifer; $E_r = \text{Revap}$ is evaporation from the shallow aquifer; Q_t is total streamflow; DA is deep aquifer; HRU is a hydrological response unit; Q_b is base flow; Q_l is lateral flow; and Q_s is surface runoff.

Watershed delineation

The current version, Arc SWAT2012 model allows the user to delineate the watershed and sub-watershed using Digital Elevation Model (DEM) interface with the Arc-GIS 10.4 and spatial analyst extension function to perform the watershed delineation. Watershed and sub-watershed delineation were carried out using various steps including DEM setup, stream definition, inlet-outlet definition, watershed outlet selection, watershed outlet definition and finally a calculation of sub-basin parameters.

Hydrological response units (HRUs)

The HRU analysis tool in Arc SWAT help to load land use, soil layers and slope map for the project. HRU analysis in SWAT includes divisions of HRUs by slope classes in addition to land cover and soils. In the model, there are two options in defining HRU distribution: assign a single HRU to each subwatershed or assign multiple HRUs to each subwatershed based on a certain threshold value. The multiple slope option (an option which considers different slope classes for HRU definition) was selected which were reclassified into five classes (namely 0-3%, 3-5 %, 5-8 %, 8-15 % and >15%). The land cover, soil and slope map should be reclassified separately in order to correspond with the SWAT database. After reclassifying the land cover, soil and slope in SWAT database, all three physical properties are overlaid for HRU definition. The fact that during model calibration optimum parameters values are established for respective HRU's (section 2.3.2) implies the application of SWAT to ungauged areas of a catchment under the condition that similarity of HRU's in gauged and ungauged areas exists. The latter applies to the Gilgel Abay area enabling to address impacts of land cover change for the (entire) Gilgel Abay.

After HRU analysis HRU definition was followed. The HRU distribution was done by assigning multiple HRU to each sub-basin. In multiple HRU definitions, a threshold level was used to reject minor land uses, soils or slope classes in each sub-basin. The SWAT user's manual suggests that a 20 % land cover threshold, 10% soil threshold and 20% slope threshold are adequate for the most modelling application. However, (Setegn et al., 2008) suggested that HRU definition with multiple options that account for 10% land use, 20% soil and 10% slope threshold combination give a better estimation of water balance components.

Therefore, for this study, HRU definition with multiple options that accounts for 10% land use, 10% soil and 5% slope threshold combination was used to get better results. These threshold values indicate that land uses which form at least 10% of the subwatershed area and soils which form at least 10% of the area within each of the selected land uses will be considered in HRU. Hence, the Gilgel Abay was divided into 13 sub-basins and 194 HRUs, each has a unique land cover, soil, and slope combinations. The number of the HRUs varies within the sub-watersheds. The selected soil service conservation curve number (SCS-CN) method for runoff simulation because it has a direct link with LC.

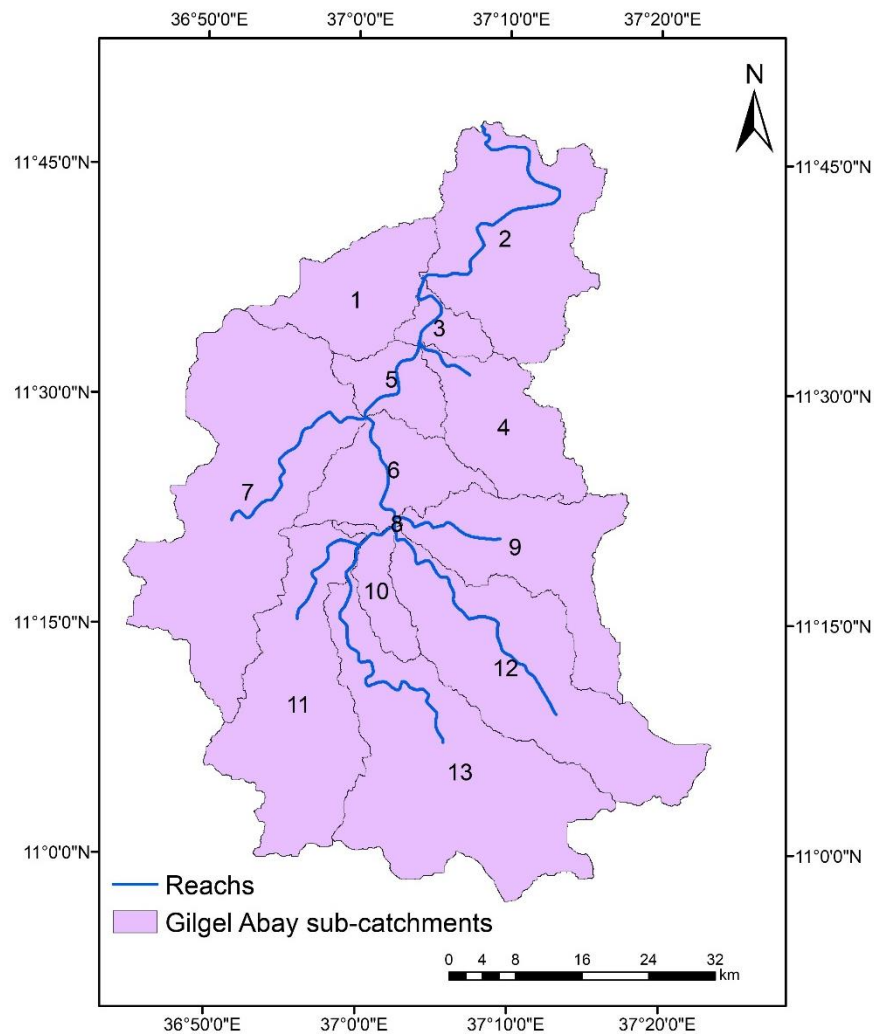


Figure 13: Gilgel Abay sub-basins, reaches

Weather data definition

It is capable of storing relevant daily weather information, easily creating txt files to be used as input information during an Arc SWAT project setup, efficiently calculating the weather statistics of several weather stations in one- step run (Essenfelder et al., 2018). Hargreaves was used to calculate reference evapotranspiration

3.2.3. Sensitivity analysis

In this study, the sensitivity analysis was carried out by using SWAT CUP. The first analysis helps to identify parameters that improve a process or characteristic of the model, while the second analysis identifies the parameters that are affected by the characteristics of the study catchment and those to which the given project is most sensitive (Abbaspour, 2015).

SWAT-CUP is used to integrate various calibration/uncertainty analysis procedures for SWAT in one user interface, make the calibrating procedure easy to use for students and experts, make the learning of the programs easier for the trainees, provide a less time-consuming calibration operations and standardize calibration steps and add extra functionalities to calibration operations such as creating graphs of calibrated results, data comparison, etc. Upon choosing a procedure, the program guides the user step by step through the input files essential for running each program. Each SWAT-CUP project contains one calibration method and allows running the procedure many times until convergence is reached. It allows saving calibration iterations in the iteration history. The eight most sensitive flow parameters are ranked in

Table 8.

Table 8: List of Parameters and their ranksss based on t-stat and p-values from SWAT cup

Parameters name	unit	Description	Range	t-stat	p-value	Rank	Significance
CN2	-	SCS runoff curve number	-0.25 to 0.25	17.92	0.00	1	Very High
ALPHA_BF	days	Base flow alpha factor	0-1	-1.07	0.32	2	High
GW_DELAY	days	Time of delay of the ground water	30-80	2.80	0.02	3	High
GW_REVAP	-	Ground water evaporation coefficient	0.02-0.2	-7.33	0.00	4	High
SOL_Z	mm	Total Soil depth	0-1	-5.85	0.00	5	High
OV_N	-	Manning's n value for overland flow	0-1	4.93	0.00	6	High
ESCO	-	soil evaporation compensation factor	0-5	-1.61	0.15	7	Medium
SOL_AWC	mm	Available water capacity of the soil layer	0-1	1.19	0.27	8	Low

3.2.4. Calibration

The calibration of the model was carried out based on the assumption that the difference between observed and simulated streamflow discharge can be minimized through optimization of model sensitive parameters. It means that all the error variance is contained in the simulated values and the measured data are free of error. But in reality, the measured data are not free of error (Arnold et al., 2012b). The SWAT cup was used for the calibration process. It took 500 simulations until it finds the best parameters set.

3.2.5. Model simulation

After achieving optimum NSE by calibrating in the baseline period, the simulation of the model is followed. The SWAT model was simulated at two outlets: at the Wetet Abay gauging station for the upper Gilgel Abay catchment and at Gilgel Abay river joining Lake Tana for the whole catchment. These simulations, which were made at Wetet Abay gauging station, aimed to assess whether a land cover change is the main driver for changes in streamflow and to test the propagation of simulation performance (NSE). The simulation periods are regarded as altered periods; the periods that the hydrological process in the catchment is predicted to be changed due to the impact of land cover changes. Two scenarios, as presented in Table 9 and Table 10, were simulated over the altered periods.

Scenario_1

Table 9. Representation of calibration without land cover change

Baseline periods	Altered periods			
1986-1994	1995-2001	2002-2008	2009-2013	2014-2018
LC1	LC1	LC1	LC1	LC1
Parameter set 1	Parameter set 1	Parameter set 1	Parameter set 1	Parameter set 1
Metrological forcing 1	Metrological forcing 2	Metrological forcing 3	Metrological forcing 4	Metrological forcing 5
1986-1994	1995-2001	2002-2008	2009-2013	2014-2018

Scenario_2

Table 10. Representation of calibration with land cover change

Baseline periods	Altered periods			
1986-1994	1995-2001	2002-2008	2009-2013	2014-2018
LC1	LC2	LC3	LC4	LC5
Parameter set 1	Parameter set 1	Parameter set 1	Parameter set 1	Parameter set 1
Metrological forcing 1	Metrological forcing 2	Metrological forcing 3	Metrological forcing 4	Metrological forcing 5
1986-1994	1995-2001	2002-2008	2009-2013	2014-2018

The SWAT simulation was also carried out at the river outlet joining Lake Tana to predict the water balance components of the whole Gilgel Abay catchment. The whole Gilgel Abay catchment consists the upper Gilgel Abay catchment (gauged at Wetet Abay station), and the downstream part of the Gilgel Abay catchment (ungauged). The calibrated parameter set at Wetet Abay was transferred for simulating the water balance components of the whole catchment, i.e., including the upper Gilgel Abay catchment and the ungauged sub-catchments. There are a number of methods for transferring parameters such as regression methods (Kokkonen et al. 2003 and Bastola et al. 2008), spatial proximity (Merz & Blöschl 2004), physical similarity (Mcintyre et al. 2005) and the areal ratio method to predict discharge in ungauged basins. Parajka et al. (2005) indicated as the regionalization method is the best in transferring model parameters. For this study, regionalization method was applied. This works at HRU level, which lumps all similar soil and land covers into a single response unit.

3.3. Attribution of change in streamflow to land cover change and climate change

According to principle of conservation of mass water balance expressed as:

$$P = Q + ET + \frac{\Delta S}{\Delta t} \quad 4$$

Where P =precipitation (mmd^{-1}), Q the discharge (mmd^{-1}) ET the actual evapotranspiration (mm d^{-1}) ΔS is change in storage (mm), and Δt the time step in all catchment. If no ΔS is assumed:

$$ET = P - Q \quad 5$$

This study states the idea of (Tomer and Schilling, 2009) who differentiate the impacts of land use and climate change on the hydrological process by using the changes in the amount of excess water relative to changes in the amount of excess energy. The amount of excess water within the system (i.e. catchment) is a result of the difference between precipitation (P) and actual evapotranspiration (ET). While the amount of excess energy is the difference in potential evapotranspiration (ET_0) and actual evapotranspiration (ET). The ratios of excess water and excess energy divided, and existing water and energy. The results are dimensionless values P_{ex} and E_{ex} on a scale of 0 to 1, mathematically stated as follows:

$$P_{ex} = 1 - ET/P \quad 6$$

$$E_{ex} = 1 - ET/ET_0 \quad 7$$

where P_{ex} is excess water, E_{ex} is excess energy, P the precipitation, ET the actual evapotranspiration and ET_0 the potential evapotranspiration. The (Tomer and Schilling, 2009) procedure follows two basic assumptions for distinguishing land use and climate change impacts on water balance components based on excess water and energy. First, LC change will affect ET , which will decrease/increase P_{ex} and E_{ex} concurrently because ET is in the numerator of both fractions. As a result, P_{ex} and E_{ex} will make an angle close to 45° or 225° with reference to the x-axis (see Figure 2.4). if there is LC change but no change with climate (i.e. $\Delta P \sim 0$ and $\Delta ET_0 \sim 0$) then the movement created at the angle of 45° indicates a decrease of water and energy consumption (e.g. decrease in ET because of decrease in the vegetated area). However, a movement creating an angle of 225° shows an increase of water and energy consumption (e.g. higher ET because of a densely vegetated area). Second, climate change has an effect P and/or ET_0 , which will be produced by a change in the ratio of P to ET_0 . If the ratio of P to ET_0 increases but ET is constant (i.e. without land cover change), the P_{ex} value will increase and/or the E_{ex} value will decrease, and vice versa, creating an angle close to 135° or 315° with reference to the x-axis (see Figure 2.4). Within the framework, a change in streamflow can be equally attributed to land cover change and climate change if movements of P_{ex} and E_{ex} are parallel to the P_{ex} axis or E_{ex} axis. A reference is made to (Tomer and Schilling, 2009) for a more detailed explanation about the concept.

Renner et al. (2014) contradict the concept of (Tomer and Schilling, 2009). According to Renner et al. (2014) the above concept cannot be practical to all hydro-climatic situations. It will work for the places where precipitation equals evaporative demand. They suggested the concept of aridity index (ET_0/P) to fix the climatic state of the study catchment. concept, a land use change impact on hydrology is defined as a change in ET , but with constant aridity, and a climate change impact on hydrology is described as changes in the average supply of water and energy. The result of P_{ex} and E_{ex} has constant aridity index is defined as a land cover change impact but the change of P_{ex} and E_{ex} not constant aridity index is considered as a climate change impact.

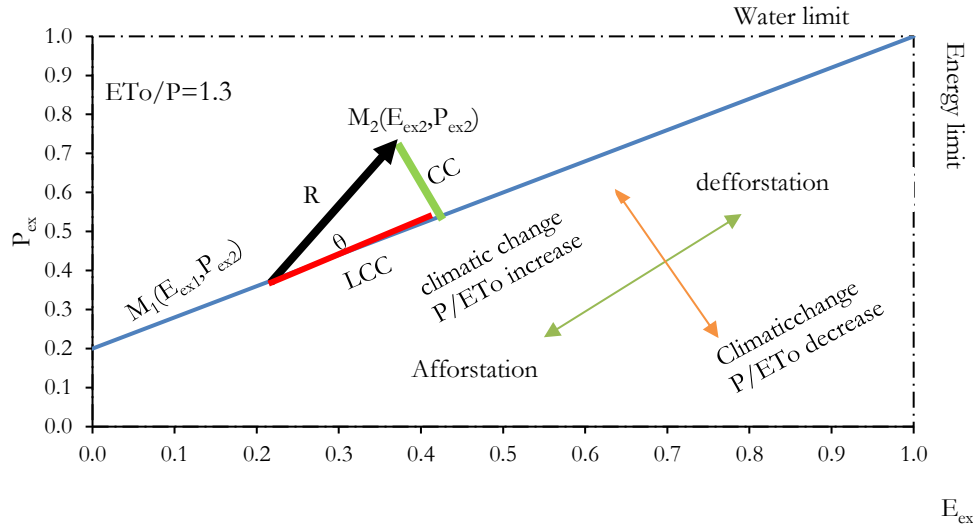


Figure 14: Framework to illustrate a fraction of excess water and energy adapted (Marhaento 2018)

For this study, the method proposed in (Renner et al., 2014) has been adapted. Defined magnitude to estimate the land cover and climate change impacts on change in streamflow and actual ET through changes of P_{ex} and E_{ex} . The duration of the analysis 1986-2018. The baseline $M_1(P_{ex1}, E_{ex1})$ and altered period, $M_2(P_{ex2}, E_{ex2})$. The following formula shows how to calculate the resultant length from M_1 to M_2 (the hypotonus) based on Pythagoras' theorem.

$$R = \sqrt{(E_{ex2} - E_{ex1})^2 + (P_{ex2} - P_{ex1})^2} \quad 8$$

Where R is the resultant length.

The angle (θ) of change indicates the contribution of land cover and climate changes with a higher slope reflecting a higher contribution of climate change. The angle (θ) can be calculated based on the gradient of the vector M_1 - M_2 relative to the gradient of the long-term aridity index using the following equations:

$$\tan \vartheta = \left| \frac{\frac{\overline{ET_0}}{\bar{P}} \frac{P_{ex2} - P_{ex1}}{E_{ex1} - E_{ex1}}}{1 + \left(\frac{\overline{ET_0}}{\bar{P}}\right) X \left(\frac{P_{ex2} - P_{ex1}}{E_{ex1} - E_{ex1}}\right)} \right| \quad 9$$

$$\theta = \arctan(\vartheta) + \pi \quad \text{if} \quad P_{ex2} < P_{ex1} + \frac{\bar{P}}{\overline{ET_0}} (E_{ex1}) - \frac{P\bar{P}}{\overline{ET_0}} (E_{ex2}) \quad 10$$

$$\theta = \arctan(\vartheta) \quad \text{if} \quad P_{ex2} > P_{ex1} + \frac{\bar{P}}{\overline{ET_0}} (E_{ex1}) - \frac{P\bar{P}}{\overline{ET_0}} (E_{ex2}) \quad 11$$

Where ϑ a ratio indicating the angle θ in radians. π is added for some cases to be able to show results in a way such that θ has a range of 2π or 360° . For this study, the second equation has fulfilled the criteria. The attribution (in %) of streamflow changes to land use change and climate change is measured by determining the length of the changes along the aridity index line and the line perpendicular to the aridity index line, which are denoted as LCC and CC respectively. The lengths of LUC and CC can be calculated as follows:

$$LCC = R * \cos \theta \quad 12$$

$$CC = R * \sin \theta \quad 13$$

The relative magnitudes of *LUC* and *CC* are denoted as *L* (%) and *C* (%) and calculated using the following equations.

$$\%L = \frac{LCC}{LCC+CC} * 100\% \quad 14$$

$$\%C = \frac{CC}{LCC+CC} * 100\% \quad 15$$

4. RESULTS

4.1. Land cover classification

Spatial analysis was carried out to develop LC map and identify the LC change of 1986, 2001, 2008, 2013 and 2018. The statistical result of LC changes was carried out for each LC maps and briefly discussed as follows.

Land cover maps

Figure 15 shows the spatial distribution of five land cover maps of Gilgel Abay catchment for 1986, 2001, 2008, 2013 and 2018. The maps have six land cover types namely agriculture, bare land, forest, grassland, residential and wetland. As mentioned in section 3.1.2, the LC maps of 2008 and 2013 were adopted from EMA, a relatively lesser process applied. These are merging and validating with GCPs.

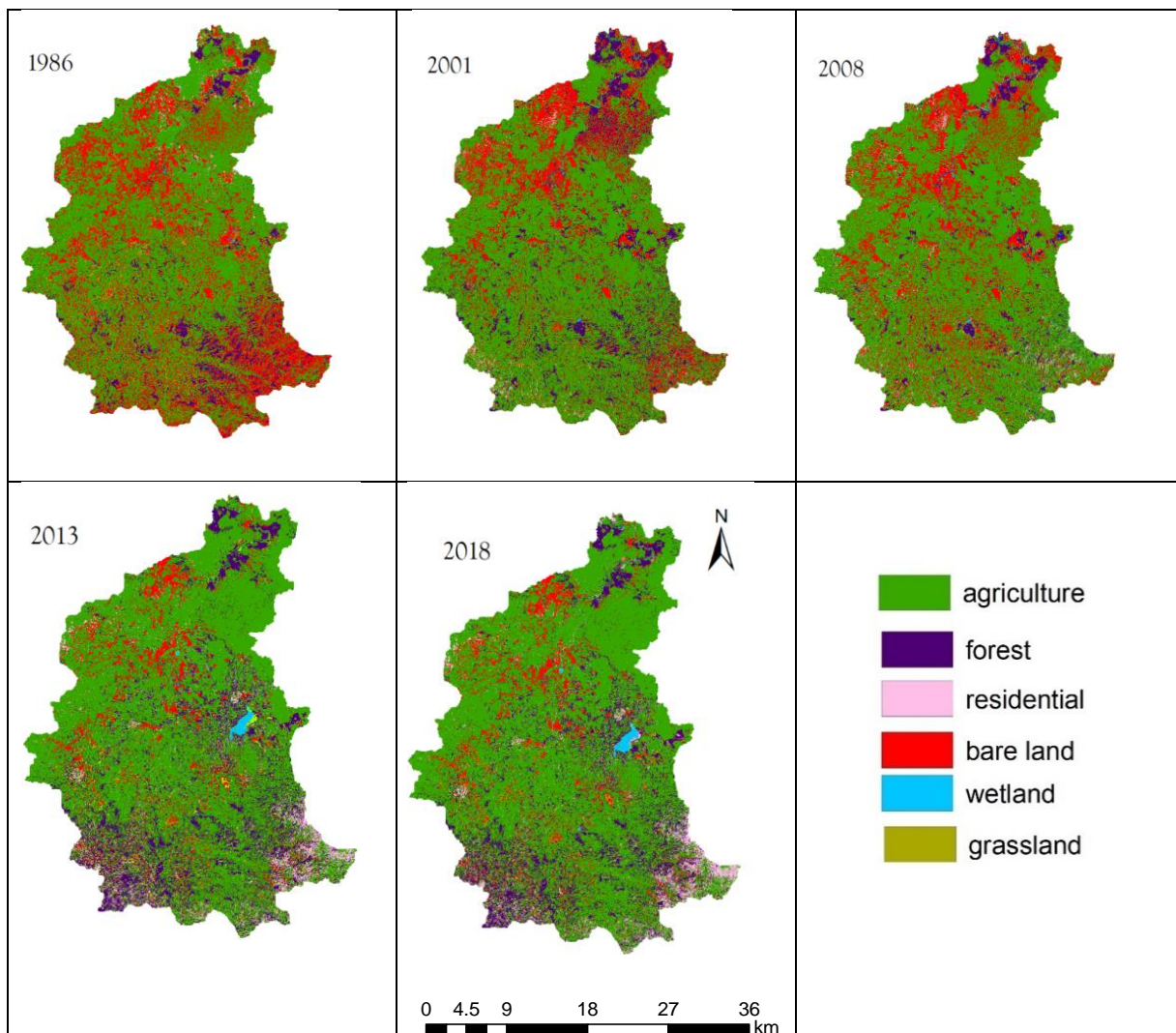


Figure 15: Land cover map of Gilgel Abay catchment for 1986, 2001, 2008, 2013 and 2018

The land cover types in % and areas are presented in Table 11 **Error! Reference source not found.** and shown in Figure 16. In 1986 the dominant land cover was agriculture 58.66% followed by bare land 26.72%, forest 8.44% and grassland 4.83 while residential area and wetland cover only 0.89% and 0.45% respectively.

After fifteen years still, agriculture is the dominant land cover but the forest for the remaining years: agriculture and forest cover 64.85% and 12.86% in 2001, 67.16% and 7.57% in 2008, 67.65% and 17.33% in 2013 and 69.40% and 15.88% in 2018.

The land covered by bare land, the second dominant in 1986 (26%), was reduced in the following years, i.e., it covers 19.13% in 2001, 20.74% in 2008, 8.06% in 2013 and 7.43% in 2018. Residential area shows expansions 1986 (0.89%) through 2018(4.98%).

The following tabulation of LC percentage and area calculations provide a comprehensive result in terms of the overall landscape, types and amount of change which had occurred (see Table 11). The growth of the agricultural area, forest coverage and residential area of all scale and categories have made a drastic change in LC all over the Gilgel Abay catchment. The grassland and bare land have been converted into Agricultural, forest and settlement areas during the entire study period (1986 to 2018).

Table 11: Summary of the land cover percentage of Gilgel Abay watershed

Individual land cover in percent and Km ²										
LC	1986		2001		2008		2013		2018	
	AREA	%_LC	AREA	%_LC	AREA	%_LC	AREA	%_LC	AREA	%_LC
Forest	316.6	8.4	482.5	12.9	284.0	7.6	650.4	17.3	595.8	15.9
Grassland	181.2	4.8	67.2	1.8	69.2	1.8	65.5	1.7	71.6	1.9
Agriculture	2201.0	58.7	2433.2	64.9	2519.9	67.2	2538.1	67.6	2603.6	69.4
Wet land	17.0	0.5	9.2	0.2	17.6	0.5	13.1	0.4	15.1	0.4
Residential	33.5	0.9	41.9	1.1	83.0	2.2	182.2	4.9	186.7	5.0
Bare land	1002.6	26.7	717.9	19.1	778.1	20.7	302.6	8.1	278.9	7.4

From the result in the Table 12, the land cover detections show the difference between the percentage of land cover of consecutive windows of LC representative window. A positive sign shows increasing the percentage, and negative sign shows decreasing of percentage. The agricultural and residential area was increasing in all window period. Forest, bare land, grassland and wetland have no consistent trend. But the overall forest was increased, while bare land, grassland and wetland were decreasing.

Table 12: change detection of land cover maps

LC types	Land cover changes (%)			
	1986-2001	2001-2008	2008-2013	2013- 2018
Forest	4.42	-5.29	9.76	-1.45
Grassland	-3.04	0.05	-0.09	0.16
Agriculture	6.19	2.31	0.49	1.75
Wet land	-0.21	0.23	-0.12	0.05
Residential	0.23	1.09	2.64	0.13
Bare land	-7.59	1.61	-12.68	-0.63

The evolution of the land cover types in certain time in percentage and Figure 16: Land cover of Gilgel Abay catchment in % (a) and km² (b)) shows land cover types coverage in a specific year in km². The larger coverage of land cover types Agriculture followed by Bare land, Forest, Residential, Grassland and wetland.

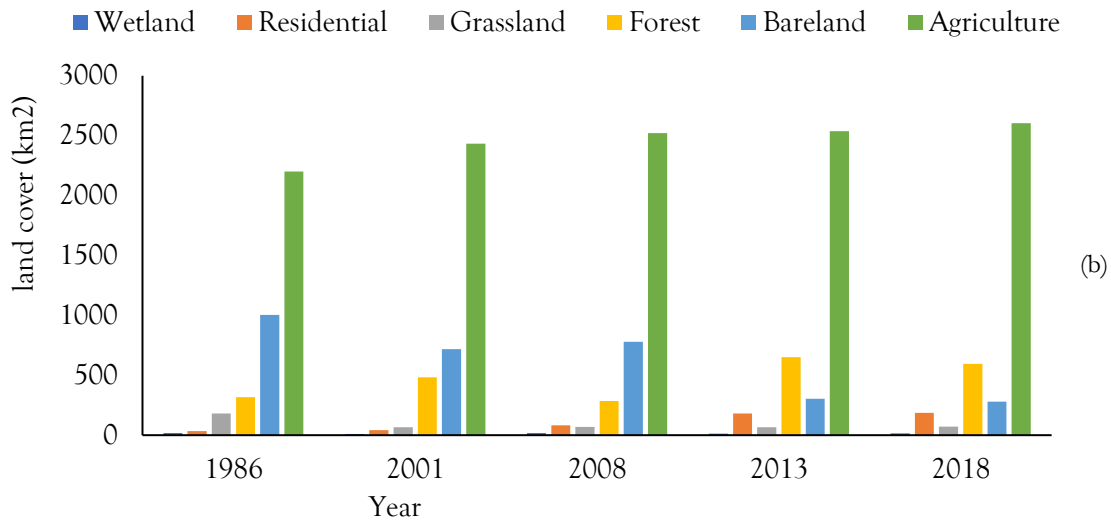
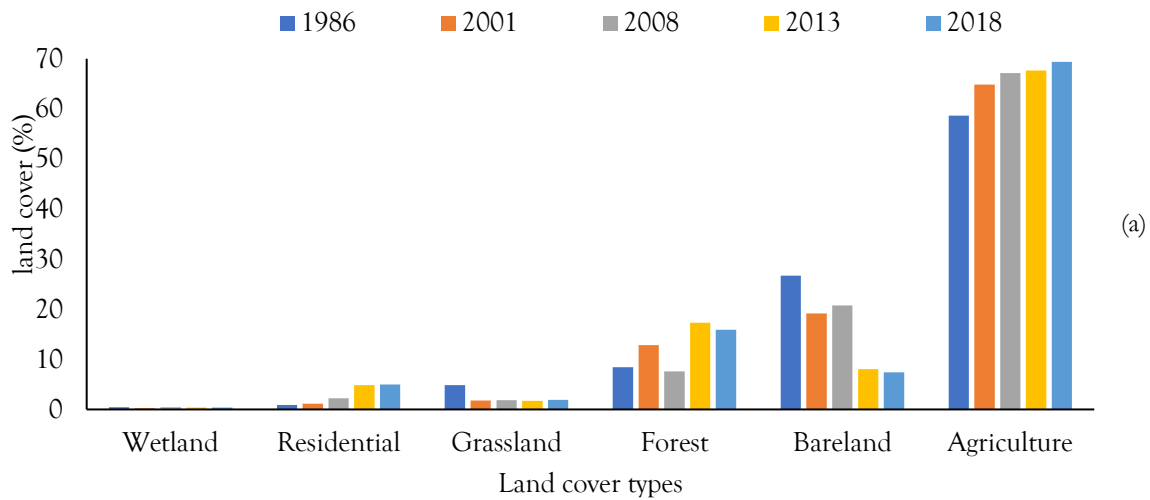


Figure 16: Land cover of Gilgel Abay catchment in % (a) and km² (b)

Confusion matrix/error matrix has numbers as the quantity of the sample. Any quantity arranged in rows and columns, i.e. square matrix, where columns represent the referencing data while row represents the classification data. The error matrix of the land cover map of 1986 calculated the parameters like the producer's accuracy, user's accuracy, overall accuracy, and kappa statistics showed in Table 13. Which is 81.46%, 83.44%, 83.01%, 81.46% and 86.09% respectively. In addition, the overall kappa coefficient for each image was 0.75 and 0.78, 0.78, 0.75 and 0.81 better agreement than by chance alone respectively.

Table 13: confusion matrix accuracy for the classified image (1986)

Classification	AGRL	BARR	FRSE	RNGE	URBN	WETL	Total	CE (%)	UA (%)
AGRL	50.00	3.00	1.00	5.00	2.00	0.00	61.00	18.033	81.97
BARR	3.00	14.00	1.00	8.00	1.00	0.00	27.00	48.148	51.85
FRSE	0.00	0.00	22.00	0.00	0.00	0.00	22.00	0.00	100.0
RNGE	2.00	0.00	0.00	28.00	2.00	0.00	32.00	12.5	87.5
URBN	0.00	0.00	0.00	0.00	6.00	0.00	6.00	0.00	100.0
WETL	0.00	0.00	0.00	0.00	0.00	3.00	3.00	100.00	0.00
Total	55.00	17.00	24.00	41.00	11.00	3.00	151.00		
OE (%)	9.09	17.65	8.33	31.71	45.45	0	Over all accuracy		81.46
PA (%)	90.91	82.35	91.67	68.29	54.55	100	sum of overlap		123.0
Kappa coefficient									0.75

BARR (Barren land), RNGE (Range Grasses), AGRL (Agricultural land generic), FRSE (Forest evergreen), URBN (Residential areas), Wetland (WETL), Omission error (OE), Commission error (CE), Producer accuracy (PA) and User accuracy (UA) and Overall accuracy (OA).

Table 14: confusion matrix accuracy for the classified image 2001

Classification	AGRL	BARR	FRSE	RNGE	URBN	WETL	Total	CE (%)	UA (%)
AGRL	50.00	3.00	1.00	5.00	0.00	0.00	59.00	15.25	84.75
BARR	3.00	12.00	1.00	3.00	3.00	0.00	22.00	45.45	54.55
FRSE	0.00	0.00	22.00	2.00	0.00	0.00	24.00	8.33	91.67
RNGE	2.00	2.00	0.00	31.00	0.00	0.00	35.00	11.43	88.57
URBN	0.00	0.00	0.00	0.00	8.00	0.00	8.00	0.00	100.00
WETL	0.00	0.00	0.00	0.00	0.00	3.00	3.00	100.00	0.00
Total	55.00	17.00	24.00	41.00	11.00	3.00	151.00		
OE (%)	9.09	29.41	8.33	24.39	27.27	0.00	Over all accuracy		83.44
PA (%)	90.91	70.59	91.67	75.61	72.73	100.00	sum of overlap		126.00
Kappa coefficient									0.75

Table 15: confusion matrix accuracy for the classified image 2008

Classification	AGRL	BARR	FRSE	RNGE	URBN	WETL	Total	CE (%)	UA (%)
AGRL	51.00	1.00	2.00	5.00	2.00	0.00	61.00	16.39	83.61
BARR	1.00	15.00	0.00	2.00	3.00	0.00	21.00	28.57	71.43
FRSE	1.00	0.00	22.00	0.00	0.00	0.00	23.00	4.35	95.65
RNGE	2.00	0.00	0.00	30.00	0.00	0.00	32.00	6.25	93.75
URBN	0.00	0.00	0.00	0.00	6.00	0.00	6.00	0	100
WETL	0.00	1.00	0.00	6.00	0.00	3.00	10.00	100	0
Total	55.00	17.00	24.00	43.00	11.00	3.00	153.00		
OE (%)	7.27	11.76	8.33	30.23	45.45	0	Over all accuracy		83.01
PA (%)	92.73	88.24	91.67	69.77	54.55	100	sum of overlap		127
Kappa coefficient									0.75

Table 16: confusion matrix accuracy for the classified image 2013

Classification	AGRL	BARR	FRSE	RNGE	URBN	WETL	Total	CE (%)	UA (%)
AGRL	50.00	3.00	1.00	5.00	2.00	0.00	61.00	18.03	81.97
BARR	3.00	14.00	1.00	8.00	1.00	0.00	27.00	48.15	51.85
FRSE	0.00	0.00	22.00	0.00	0.00	0.00	22.00	0.00	100.00
RNGE	2.00	0.00	0.00	28.00	2.00	0.00	32.00	12.50	87.50
URBN	0.00	0.00	0.00	0.00	6.00	0.00	6.00	0.00	100.00
WETL	0.00	0.00	0.00	0.00	0.00	3.00	3.00	100.00	0.00
Total	55.00	17.00	24.00	41.00	11.00	3.00	151.00		
OE (%)	81.46	17.65	8.33	31.71	45.45	0.00	Over all accuracy		83.44
PA (%)	123.00	82.35	91.67	68.29	54.55	100.00	sum of overlap		126.00
Kappa coefficient									0.75

Table 17: confusion matrix accuracy for the classified image 2018

Classification	AGRL	BARR	FRSE	RNGE	URBN	WETL	Total	CE (%)	UA (%)
AGRL	50.00	3.00	1.00	5.00	2.00	0.00	61.00	18.03	81.97
BARR	3.00	13.00	1.00	0.00	1.00	0.00	18.00	27.78	72.22
FRSE	0.00	1.00	22.00	0.00	0.00	0.00	23.00	4.35	95.65
RNGE	2.00	0.00	0.00	36.00	2.00	0.00	40.00	10.00	90.00
URBN	0.00	0.00	0.00	0.00	6.00	0.00	6.00	0.00	100.00
WETL	0.00	0.00	0.00	0.00	0.00	3.00	3.00	100.00	0.00
Total	55.00	17.00	24.00	41.00	11.00	3.00	151.00		
OE (%)	9.09	23.53	8.33	12.20	45.45	0.00	Over all accuracy		86.09
PA (%)	90.91	76.47	91.67	87.80	54.55	100.00	sum of overlap		130.00
Kappa coefficient									0.81

The overall accuracy for the LC of 1986, 2001, 2008, 2013 and 2018 images was defined as the total correct pixels (major diagonal's sum) divided by the total number of pixels in the provided matrix. The Kappa coefficient for the years 1986, 2001, 2008, 2013 and 2018 was calculated. These values show substantial agreement. Table 18, shows the results of the kappa coefficient of each corresponding years of land cover maps.

Table 18: Kappa coefficient values

Years	Overall accuracy	Kappa coefficient
1986	81.46	0.75
2001	83.44	0.78
2008	83.01	0.78
2013	82.33	0.75
2018	86.09	0.81

4.2. Calibration of the SWAT model

Calibration was done for the eight years' period from 1986 –1994 with three years for warming the model was performed. For the simulated results based on the sensitive parameters ranked in

Used for calibration at monthly time step using Sequential Uncertainty Fitting program (SUFI). It has been described by SWAT term to describe eight SWAT parameters were calibrated, namely CN2, GW_REVAP, SOL_AWC, ESCO, SOL_Z, GW_DELAY, ALPHA_BF and CANMX. CN2 is the curve number parameter, for monitoring the fraction of water to infiltrate into the soil or to produce surface runoff from overland flow as CN is larger reason for lesser infiltration which increases the surface runoff. SOL_AWC is the available water capacity of the soil layer. It monitors the soil water storage from field capacity and permanent wilting point of the soil moisture. GW_DELAY is a time of delay of the groundwater and it is monitoring delay time between water leaving from soil layers and enter the shallow aquifer. As GW_DELAY increases evaporation from the unsaturated zone will increase. GW_REVAP has two functions. The first groundwater revap coefficient is the movement of water in the zone of unsaturated which will be used for water demand for evapotranspiration. The second function GW_REVAP parameter controls the water movements in the capillary fringe which is a boundary between the unsaturated zone and the saturated zone to fulfil the demand for evaporative. As GW_REVAP increases the transmission rate from the shallow aquifer to the unsaturated zone will increase.

ESCO is the evaporation from the soil compensation factor which controls the demand of evaporation of the soil. To fulfil evaporative demand from the lower soil level for specific model ESCO should be closer to zero. ALPHA_BF, Baseflow alpha factor (days) controls groundwater flow response to changes in recharge (Smedema and Rycroft, 1983). As ALPHA_BF larger the lesser baseflow factor. Soil depth (SOL_Z) is a depth from the soil surface to bottom layer. CANMX is the maximum canopy stored to intercept precipitation. OV_N Manning's "n" value for overland flow roughness coefficient. OV_N controls the time of concentration and slope of the overland flow; the larger the OV_N the lesser overland flow is.

For manual calibration parameters, CN2 and SOL_AWC, were scaled at HRU level and Calibrated. The default parameter value was multiplied by 1 (+/the scaled parameter values). Default parameters will stay with their original distribution pattern. Parameter values are consistent for the whole catchment. For this study, Calibration took five iterations to get finest calibrated hydrograph of baseline period value with an NSE value of 0.83 (see Figure 17).

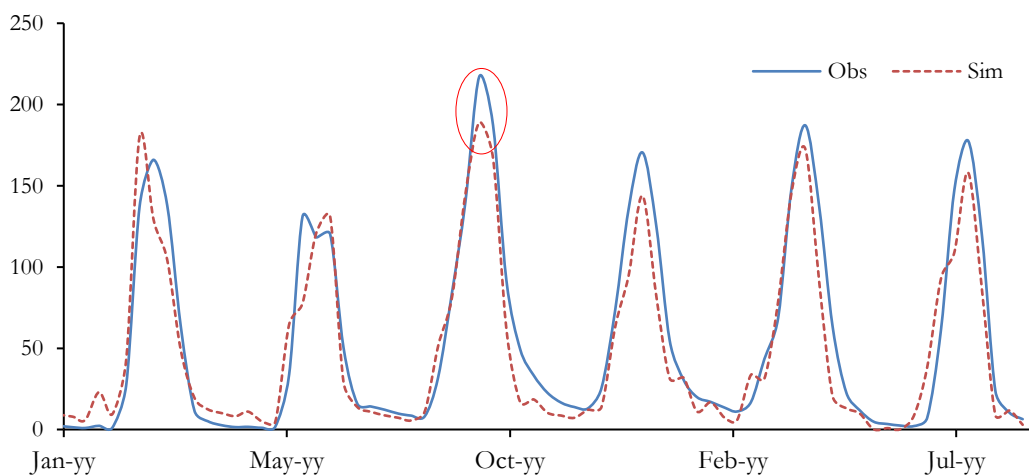


Figure 17: Simulated hydrograph of the base period

Error! Not a valid bookmark self-reference. shows the calibrated parameter values used in this study. The deviation of the peak flow of observed and simulated discharge hydrograph in 1991 presumably results

from poor observations or use of inadequate stage-discharge relationship or might be bigger attention was paid for the water balance calibration than the shape of the hydrograph.

Table 19: Summary of the calibrated value of flow parameters

Parameters				Calibrated
Name	Unit	Description	Range	Value
CN2	-	SCS runoff curve number	- 0.25 to 0.25	0.17
GW_REVAP	-	Ground water evaporation coefficient	0.02-0.2	0.19
SOL_Z	mm	Total Soil depth	0-1	0.76
OV_N	-	Manning's n value for overland flow	0-1	0.04
GW_DELAY	days	Time of delay of the groundwater	30-80	52
ESCO	-	soil evaporation compensation factor	0-5	3
SOL_AWC	mm	Available water capacity of the soil layer	0-1	0.16
ALPHA_BF	days	Base flow alpha factor	0-1	0.70

Note (-) Means no unit

4.3. Performance of the model with and without LC update

After calibrating manually and getting 0.83 values of NSE for baseline period stream flow for nine years period from 1986–1994, the simulation was performed to altered periods (1995–2001, 2002–2008, 2009–2013 and 2014–2018) without changing the calibrated parameter set values. The model performance evaluation criteria the flow calibration and simulation for the Gilgel Abay catchment using 1986–2018 LC update showed a very good performance than without LC update. There NSE of value for altered periods with and without LC update is for AP1, 0.78 and 0.75, NSE of AP2 is 0.76 and 0.68, NSE of AP3, 0.74 and 0.4 and finally, AP4 is 0.69 and 0.28 respectively.

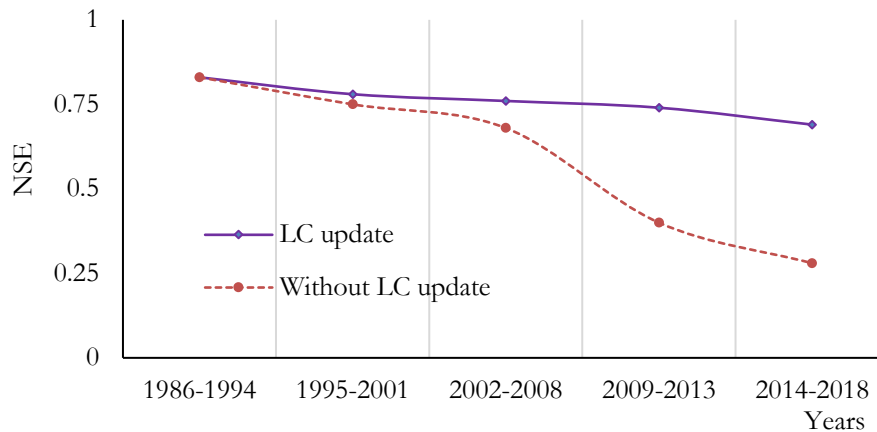


Figure 18: Figure 14: Model performance, Nash-Sutcliffe efficiency with and without LC changes

The model performance for simulations with and without LC update are shown in Figure 19 for altered periods (1995–2016). For the altered periods the results of the simulations without LC update shows

decreasing NSE value up to the end of the altered period, with a slight decrease in the AP1. The simulation performance (NSE values) of the altered periods (1,2,3, and 4) have better NSE with LC update than without LC update. Both simulated peak flows and low flows of the simulations with LC update are better than in the simulations without the LC update. The mean NSE value of simulations with and without LC update over the altered periods are 0.76 and 0.58 respectively.

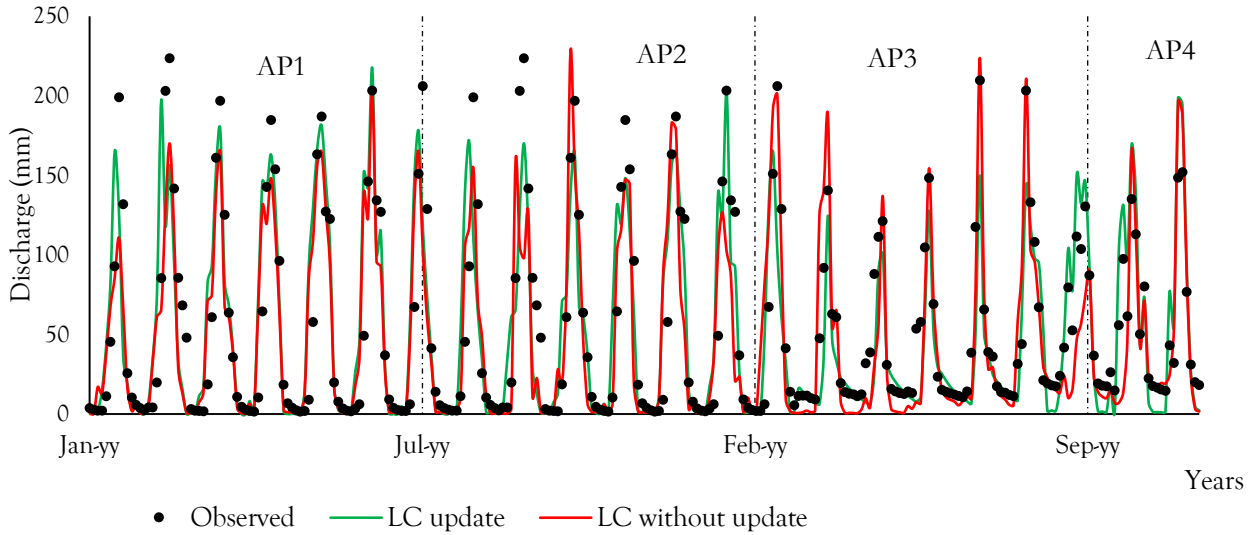


Figure 19: Hydrograph of observed and simulated discharge with and without the land cover update for the altered period 1, 2, 3 and 4.

Figure 20 shows the hydrograph of observed and simulated discharge with a land cover update for the altered period 1 to 4. In the figure the simulated flows well-fitted the observed discharge but that the peak values were unable to catch.

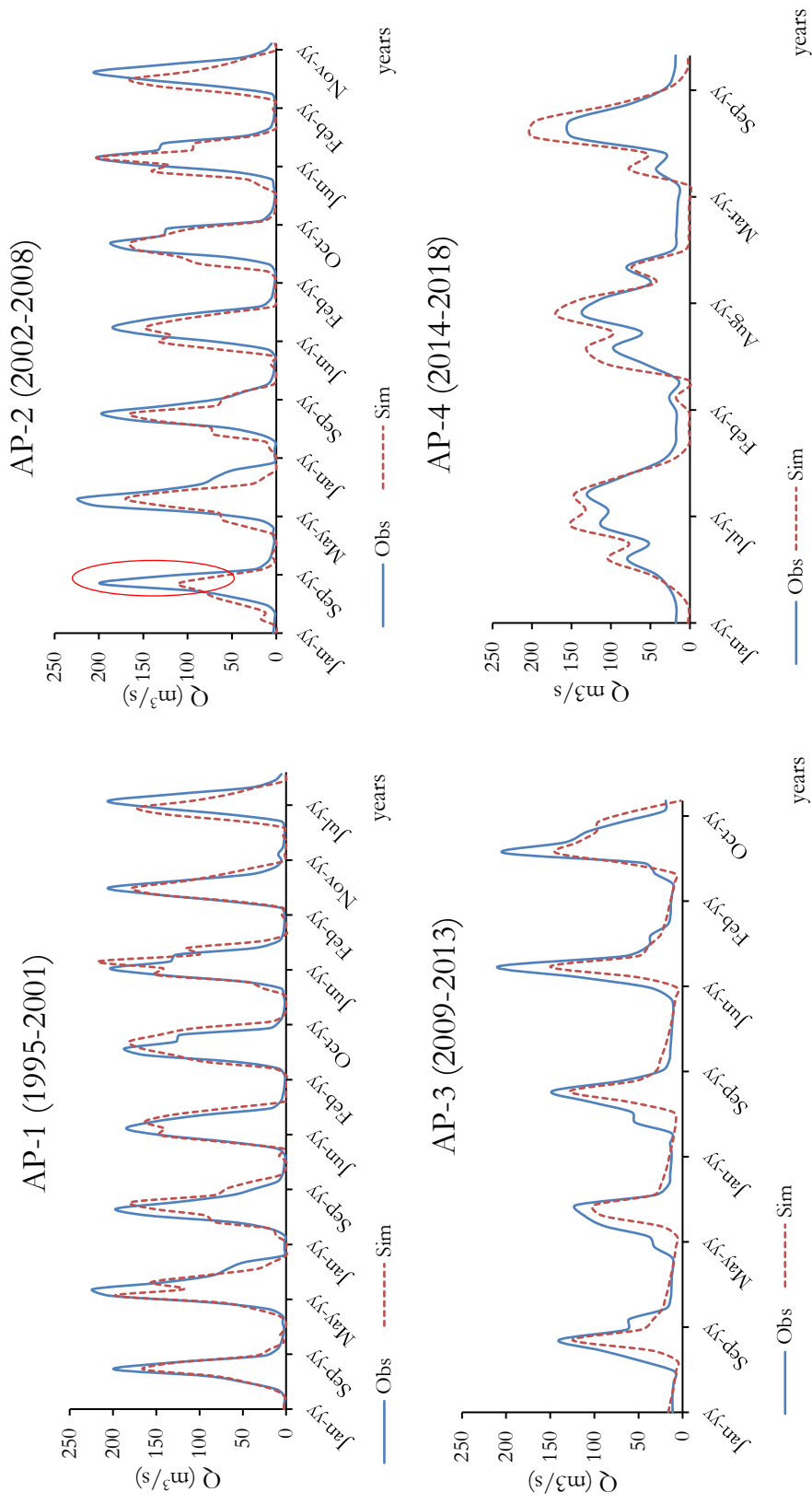


Figure 20: Hydrograph of observed and simulated discharge with land cover update for the altered period 1, 2, 3 and 4.

4.4. Effect of land cover change on water balance component

The outcomes of the simulation with the LC update showed that the water balance of the catchment has altered within 30-years. Table 20 shows the mean annual water balance components per window periods.

Table 20: Mean annual water balance components in (mm)

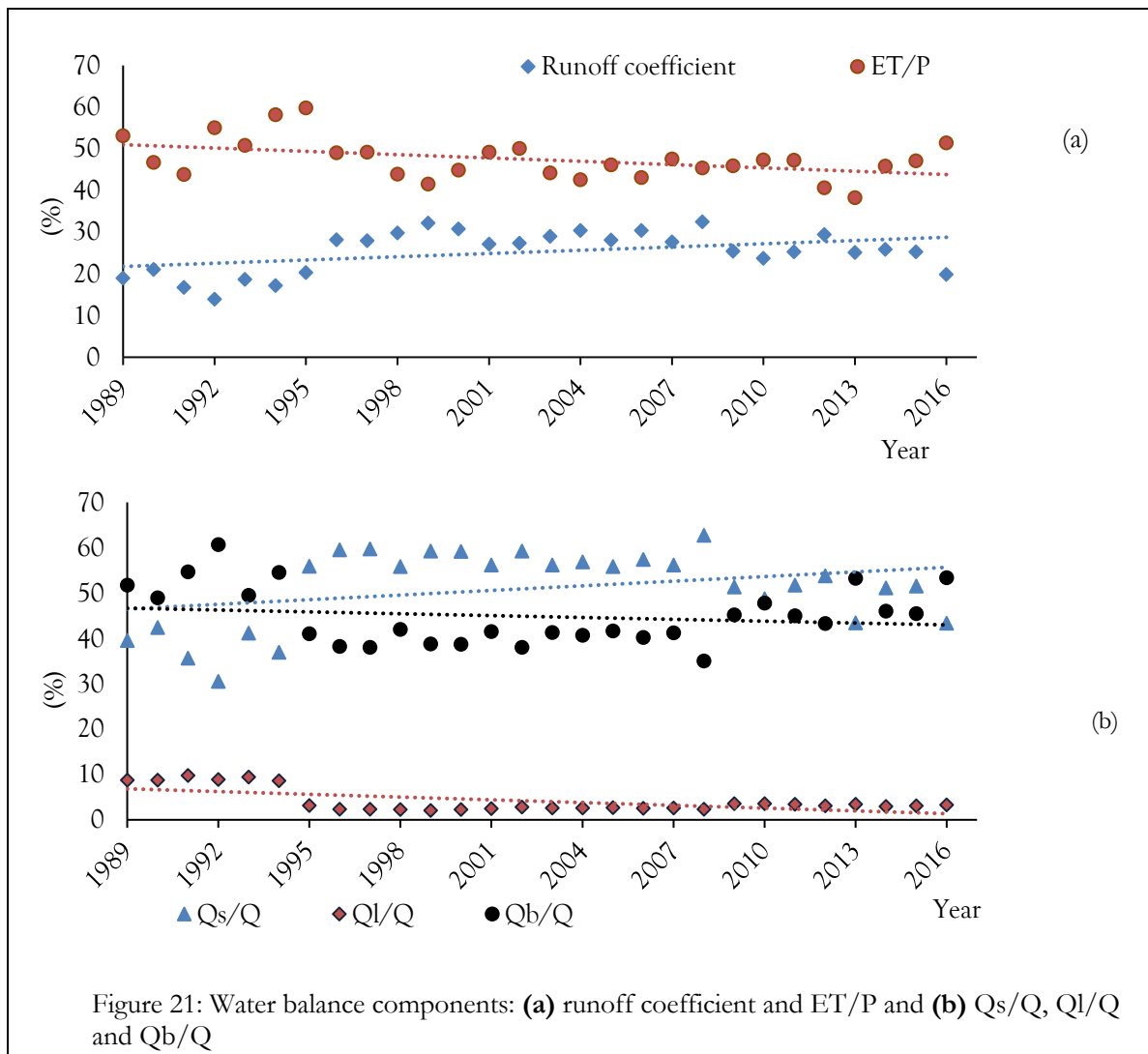
Years	Rainfall	Qs	Ql	ET	Qb	Streamflow
1986-1994	1343	121	66	685	471	658
1995-2001	1365	388	15	649	313	716
2002-2008	1320	389	17	599	315	721
2009-2013	1360	348	23	614	375	746
2014-2016	1522	361	23	731	407	791

Table 21: Summary of water balance components ratio in percentage

Water balance component (%)	BL 1986-1994	AP-1 1995-2001	AP-1 2002-2008	AP-2 2009-2013	AP- 4 20014-2018
Streamflow/precipitation	56	49	51	51	49
Baseflow/stream flow	62	42	42	50	51
Surface runoff/streamflow	38	58	58	50	49
ET/precipitation	40	48	45	45	48

Figure 21(a) shows the effects of land cover change on water balance components. Runoff coefficient (Q/P) and ET/P their long-term trend for the period 1986-2016 with three years for warming period in the Gilgel Abay catchment. Their trendline shows decreasing values for ET/P but increasing values for Q/P . Figure 21(b) shows Q_s/Q , Q_b/Q and lateral discharge/streamflow (Q_l/Q). This shows Q_s/Q increases, that Q_b/Q slightly decreases, and that Q_l/Q decreases over respective At the catchment level, showed the changes in the runoff coefficient and ET/P were significant. Comparing BL and AP4, the runoff coefficient has decreased from 56% to 49%, and ET/P has increased from 40% to 48%. Nevertheless, for the ratio of mean annual streamflow to precipitation (Q/P) shows a slight increasin trend whereas values for ET/P a slight decreasing trend is shown in Figure 21.

Regardless of changes in Q_s/Q and Q_b/Q between BL and AP4, Q_s/Q has increased from 38% to 49% while Q_b/Q has decreased from 62% to 51%.



4.5. Attribution of change in streamflow to land cover change and climate change

The method for attributing the change in streamflow and actual ET to land cover change and climate change was adapted from the (Renner et al., 2014). Renner et al. (2014) defined the method to estimate the land cover and climate change impacts on the change in streamflow through changes of P_{ex} and E_{ex} . The magnitude of the resultant of the change is between the baseline $M_1 (P_{ex1}, E_{ex1})$ and altered period, $M_2 (P_{ex2}, E_{ex2})$.

Figure 22 shows the results of the change of excess water and excess energy in relative to long term aridity index line. According to Marhaento, (2018) the downward arrow shows the afforestation of the land cover. The attribution of streamflow and actual ET were calculated as 86% from land cover change and 14% from climate change. So, this result justifies that the change in streamflow and actual ET is mostly caused by land cover change than climate change.

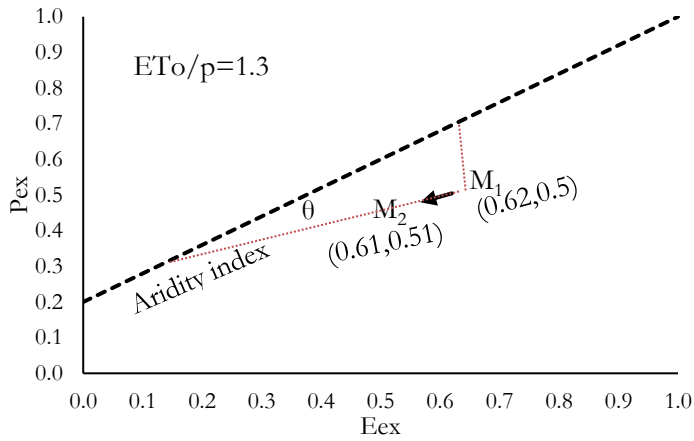


Figure 22: Change of excess water and excess energy in relative to long term aridity index line

Table 22: Measure of the attribution streamflow alteration to LC change and climate change

Period	P	Q	ET	E _{to}	P _{ex}	E _{ex}	R	θ	LCC	CC
Base	1365.11	688.96	676.17	1778.44	0.5	0.62				
Altered	1387.75	712.85	674.91	1784.67	0.51	0.61	0.06	37	86	14

The calculated angle is 37° which is less than 45° signifying the climate change (P and ET_0) is slight and has a lesser influence than land cover changes on the streamflow change. Moreover, the change of P_{ex} and E_{ex} has quite low Resultant value (R) of 0.06. The result showed that the mean annual precipitation (1486mm) significantly changed and mean annual potential evapotranspiration (1781mm) have slightly changed. While the mean annual discharge has changed significantly. The results are in line with the attribution results, which generally revealed a small contribution of climate change to changes in streamflow.

5. DISCUSSION

In this study, the effect of LC changes between 1886 and 2018 on actual evapotranspiration and streamflow in Gilgel Abay catchment are assessed. Preparation of LC maps and assessment of the land cover changes were made using three remote sensing images of Landsat for 1986, 2001, 2018 acquired in the dry season (i.e., January) and two LC maps for 2008 and 2013 from Ethiopian mapping agency. Five LC maps are prepared by applying a supervised classification method by considering six LC types. Those are agriculture, bare land, grassland, forest, wetland and residential areas. The accuracy assessment is done by using a confusion matrix that assesses the producer's accuracy, user's accuracy, overall accuracy and the kappa statistics. The overall accuracy of generating the LC map of 1986, 2001, 2008, 2013 and 2018 are 81.46%, 83.44%, 83.01%, 81.46% and 86.09% respectively. The respective kappa coefficient of the land cover map classification is calculated to be 0.75, 0.78, 0.78, 0.75 and 0.81; the value of the kappa coefficients confirms substantial agreement between the classified and surveyed land cover types.

The land cover change was assessed by comparing the land cover map of 2018 to the reference land cover map of 1986. Between 1986 and 2018, agriculture land cover expanded from 58.66 % in 1986 to 69.4% in 2018, and settlement from 0.89% in 1986 to 4.98% in 2018. In the same period, grassland and bare land decreased by 2.92% and 19.29% respectively. Our result that agricultural and settlement land increased is consistent with the finding in Rientjes et al., (2011), but the magnitude of LC changes are different. This is because Rientjes et al., (2011) assessed the land cover changes for the upper Gilgel Abay and in the period from 1986 to 2001. In this study, the expansion of forest cover from 8.44% in 1986 to 15.88% in 2018 is identified. What seems to contradict to the finding in the current study is the assessment in Rientjes et al. (2011), which reports decreasing forest cover from 32.9 % to 16.7 % in the period 1986–2001. However, Rientjes et al., (2011) observed a decreasing rate of deforestation and ongoing afforestation activities towards the end of their study period (2001). Two common practices can explain the detected expansion of forest cover in the watershed. Watershed management measures such as area closure, which involves the protection and resting of degraded land, has been implemented in the area (Chanje et al., 2013). The plantation of eucalyptus trees for economic benefit is also increasing in the catchment (Enku et al., 2014) can be the reason for the expansion of forest cover in the catchment. In the current study, the relatively large increase in the forest and agriculture land cover is observed in the upper part of the catchment and around the catchment outlet to the Lake Tana.

Parameterisation is most challenging in model development and simulation. Selection of parameters to be calibrated is important for the model process. In this study, eight sensitive parameters that are CN2, GW_REVAP, SOL_AWC, ESCO, SOL_Z, GW_DELAY, ALPHA_BF and CANMX. have been selected for calibration in the baseline period from 1986 to 1994. These parameters are fine-tuned automatically and manually until the best fit between simulated and observed streamflow are observed. Nash Sutcliffe efficiency (NSE), the indicator to measure the simulation performance, is calculated 0.83 for the baseline period.

In the current study, the propagation of SWAT simulation performance in five consecutive window periods is analysed. The outcome of our analyses confirms the hypothesis, which was developed following the finding of Marhaento et al. (2017). Our analyses confirm the hypothesis that the simulation performance of the SWAT model is better with LC update than without the LC update. The NSE values of the altered periods (1,2,3, and 4) have consistently higher values than the NSE without LC update. It is also confirmed that the NSE decreases from the baseline period through the first to the fourth altered period. With the land cover update, the NSE for AP1 through AP4 are 0.78, 0.76,

0.74, and 0.69. Without LC update, the NSE for AP1 through AP4 are 0.75, 0.68, 0.4 and 0.28. Thus, the result showing LC update increasing model performance than simulations without LC update confirms the finding of Marhaento et al. (2017).

The increases in agricultural land and forest cover and the decrease in bare land and grassland in Gilgel Abay catchment are the dominant land cover changes that cause the change on water balance components. The effect of land cover and climate changes between 1986 to 2018 causes changes to water balance components (see Figure 23). The runoff coefficient, $\sum \text{Runoff}/Q$, increases from 38% in the baseline period to 58% in altered period 3 (AP3) then decrease to 49% in AP4. The ratio of actual evapotranspiration to precipitation, $\sum \text{ET}/P$, increases from 40% in AP1 to 48% in AP4. The ratio of runoff to precipitation ($\sum Q/P$) decreases from 56% in the baseline period to 49% in AP4. Baseflow fraction, the ratio of baseflow to streamflow (Q_b/Q), decrease from 62% in AP1 to 42% in AP3 and then increase to 51% in AP4. Following the reduction of bare land and grassland coverage and expansion of agricultural and forest cover, a decrease in runoff and increase in ET was expected; however, the increase in ET and runoff are detected. The land cover changes due to the expansion of agricultural areas and settlement areas are probably the cause of significant changes in streamflow generation. As the result of the attribution outcomes, the changes in streamflow and actual ET can be largely attributed to land cover changes rather than to climate change in the Gilgel Abay catchment. The land cover changes between 1986-2018 attributed to 86% of the streamflow change in Gilgel Abay flow to Lake Tana. This also since changes in the climate as indicated by slight changes in annual ET_0 and P is minimal.

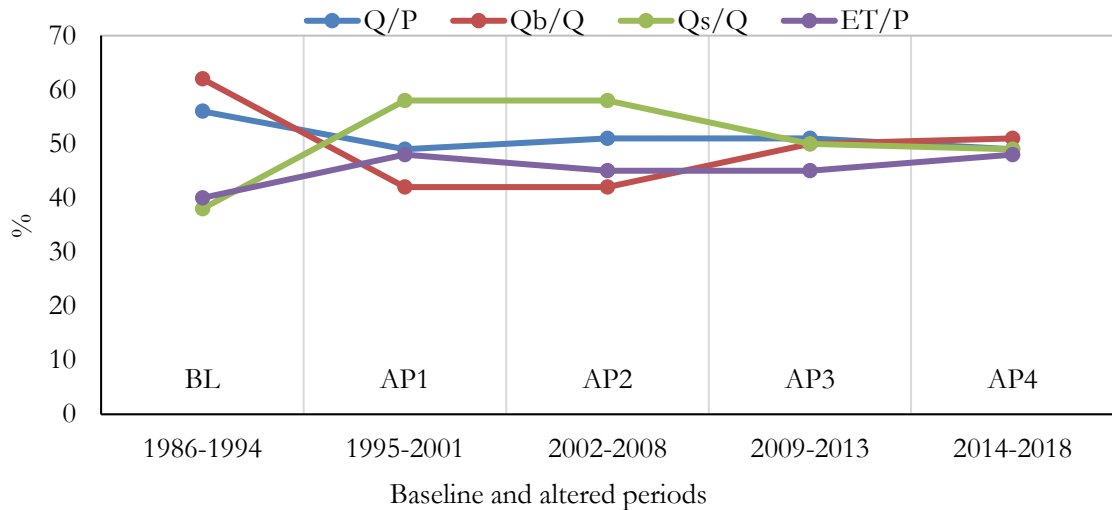


Figure 23: The ratio of water balance components in baseline and altered periods

To accomplish the research objectives, this research used several datasets such as spatial data (e.g. satellite images, elevation data and soil data) and non-spatial data (e.g. hydro-meteorological data). The available climatic data (precipitation, minimum and maximum temperature) are from 1986-2016. These meteorological stations are, however, few and they are not evenly distributed across the catchments. Finding long-term hydrological data was a challenge for the study; the observed discharge at Wetet Abay is only from 1986 to 2008. Discharge data, which were synthesised by simulating using the SWAT model, are used to represent the observed data from 2009 to the end of the simulation period.

Additionally, this study applied a hydrological model to assess the impacts of land cover change on hydrological processes using daily climatic data and one land cover map representing per a window period. The land cover reflects only a specific date and year; this could affect the simulated water

balance components particularly for ungauged part of the catchment where a reservoir is observed. In the ungauged part of Gilgel Abay catchment (downstream of Wetet Abay), the reservoir of Koga dam is detected on the land cover map of 2013 and 2018. Our simulation, however, does not consider reservoir operation and irrigation schemes, which can alter the result of the simulated water balance components.

Uncertainties due to the input data, transferring of the model parameter from upper Gilgel Abay catchment to serve for the whole catchment and inherent limitation in the SWAT model put disclaimers on the results of our study. This can also lead to uncertainty in the overall water balance (Montanari and Di Baldassarre 2013; van den Tillaart et al. 2013). The study is also done in a limited time and resource. Thus, caution should be taken in interpreting and applying the findings. The methods and the finding of the current study can be used as a starting point for further studies.

6. CONCLUSION

Assessing the change in land cover and how such changes affect the water balance components is vital for water resource management particularly in areas such as Gilgel Abay catchment where the water demand is rising. In this study, the propagation of SWAT simulation performance from 1986 through 2018 divided into five window periods are evaluated considering without and with the land cover update. After quantifying the land cover changes in these five periods, the effect of the land cover changes on water balance components was assessed using the SWAT model. Three main conclusions in this study are:

- The result of LC change detection of the Gilgel Abay river basin indicated that the agricultural land holds the dominant portion of the basin 58.66 % and 69.4% in 1986 and 2018 respectively. From the land cover change analysis, it can be concluded that Gilgel Abay catchment had experienced a significant LC change over the past three decades. The dominant land cover changes are the expansion of agriculture from 58.66 % in 1986 to 69.4% in 2018, forest coverage from 8.44 % in 1986 to 15.88% in 2018 and residential settlement from 0.89% in 1986 to 4.98% in 2018. These land cover changes are at the expense of the reduction of bare land and grassland coverage.
- A calibrated SWAT (NSE of 0.83) for the baseline period (1986-1994) is applied to investigate the propagation of simulation performance in four altered periods from 1986-2018 with and without the land cover update. The simulation performance (NSE values) continuously decrease with and without land cover changes from the baseline periods to altered period 4. Thus, it is concluded that simulation performance is better with the LC update than without the LC update. It is also concluded that the simulation performances (NSE values), from the baseline periods to altered period 4, decrease at a slower rate with LC update than without land cover update.
- The effect of land cover on water balance components was separated from the combined effect of land cover and climate change on water balance components. It is concluded that 86% the change in streamflow in the Gilgel Abay catchment during the period 1986–2018 attributed to LC change and 14% to climate change. It was also noticed that the expansion of both agricultural and forest coverage and climate change affect the runoff and ET components of the water balance; the expansion of agriculture tends to increase runoff and decrease ET but the expansion of forest does the opposite. Together with the effect of climate change from 1986-2018, it was calculated an increase in surface runoff due to the effect of agriculture, the dominant land cover holding about 69.4% of the catchment and increase in ET due to increasing of forest coverage. But ET/P decreased because the effect of the change in agricultural land is greater than the effect of forest expansion.

LIST OF REFERENCES

- Abbaspour, K. C. (2015). *SWAT-CUP SWAT Calibration and Uncertainty Programs*. Retrieved February 16, 2019, from <https://swat.tamu.edu/media/114860/usermanual_swatcup.pdf>
- Abebe. (2005). *Diversity in homestead agroforestry systems of Southern Ethiopia*. Retrieved November 22, 2018, from <<https://library.wur.nl/WebQuery/wurpubs/fulltext/121644>>
- Ajayi. (2004). *Pakistan journal of scientific and industrial research. Series B, Biological sciences. Pakistan Journal of Scientific and Industrial Research (Pakistan)*. Scientific Information Center, Pakistan Council of Scientific and Industrial Research.
- Arnold, J. G., Moriasi, D. N., Gassman, P. W., Abbaspour, K. C., White, M. J., Srinivasan, R., Santhi, C., et al. (2012). 'SWAT: MODEL USE, CALIBRATION, AND VALIDATION', *Transactions of the ASABE*, 55/4: 1491–508.
- Bastola, S., Ishidaira, H., & Takeuchi, K. (2008). 'Regionalisation of hydrological model parameters under parameter uncertainty: A case study involving TOPMODEL and basins across the globe', *Journal of Hydrology*, 357/3–4: 188–206. Elsevier. DOI: 10.1016/J.JHYDROL.2008.05.007
- Chanie, T., Collick, A. S., Adgo, E., Lehmann, J., & Steenhuis, T. S. (2013). 'Eco-hydrological impacts of Eucalyptus in the semi humid Ethiopian Highlands: the Lake Tana Plain', *J. Hydrol. Hydromech*, 61/1: 21–9. DOI: 10.2478/johh-2013-0004
- Chen, Z. Q., Kavvas, M. L., Fukami, K., Yoshitani, J., & Matsuura, T. (2004). 'Watershed Environmental Hydrology (WEHY) Model: Model Application', *Journal of Hydrologic Engineering*, 9/6: 480–90. DOI: 10.1061/(ASCE)1084-0699(2004)9:6(480)
- Congalton. (1990). *Photogrammetric engineering and remote sensing. PE&RS, Photogrammetric Engineering & Remote Sensing*, Vol. 56. American Society of Photogrammetry.
- Devia, G. K., & Ganasri, B. P. (2015). 'A Review on Hydrological Models', *Aquatic Procedia*, 4: 1001–7. Elsevier. DOI: 10.1016/J.AQPRO.2015.02.126
- Eastman, J. R. (2001). *Guide to GIS and Image Processing Volume 1 Release 2*. Retrieved November 22, 2018, from <http://planet.uwc.ac.za/nisL/GIS/IDRISI/Idrisi32Tutorial/Documents/Idrisi_Guide1.pdf>
- Enku, T., Tadesse, A., Yilak, D., Gessesse, A., Addisie, M., Abate, M., Zimale, F., et al. (2014). 'Biohydrology of low flows in the humid Ethiopian highlands: The Gilgel Abay catchment', *Biologia*, 69/11. DOI: 10.2478/s11756-014-0462-9
- Eshleman, K. N. (2004). 'Hydrological consequences of land use change: A review of the state-of-science'. *Geophysical Monograph Series*. DOI: 10.1029/153GM03
- Essenfelder, A. H., Pérez-Blanco, C. D., & Mayer, A. S. (2018). 'Rationalizing Systems Analysis for the Evaluation of Adaptation Strategies in Complex Human-Water Systems', *Earth's Future*, 6/9: 1181–206. John Wiley & Sons, Ltd. DOI: 10.1029/2018EF000826
- Fisher, J. I., & Mustard, J. F. (2004). 'High spatial resolution sea surface climatology from Landsat thermal infrared data', *Remote Sensing of Environment*. DOI: 10.1016/j.rse.2004.01.008
- Fonji, S., & Taff, G. N. (2014). 'Using satellite data to monitor land-use land-cover change in North-eastern Latvia', *SpringerPlus*, 3/1: 61. Springer International Publishing. DOI: 10.1186/2193-1801-3-61
- Gayathri, D. K., Ganasri, P. B., & Dwarakish, S. G. (2015). 'International conference on water resources, coastal and ocean Engineering (ICWRCOE 2015)',
- Gumindoga. (2014). 'Predicting streamflow for land cover changes in the Upper Gilgel Abay River Basin, Ethiopia: A TOPMODEL based approach', *Physics and Chemistry of the Earth, Parts A/B/C*, 76–78: 3–15. DOI: 10.1016/j.pce.2014.11.012
- Herbert F. Wang. (2017). 'Theory of Linear Poroelasticity with Applications to Geomechanics and'. Retrieved November 21, 2018, from <[https://books.google.nl/books?hl=en&lr=&id=4GfVDQAAQBAJ&oi=fnd&pg=PP1&dq=\(Wang+etal.,+2017&ots=xfupQgB23p&sig=zmb8C7xv3wzlCCalDHX34k0tfHs#v=onepage&q=\(Wang+etal.%2C+2017&f=false](https://books.google.nl/books?hl=en&lr=&id=4GfVDQAAQBAJ&oi=fnd&pg=PP1&dq=(Wang+etal.,+2017&ots=xfupQgB23p&sig=zmb8C7xv3wzlCCalDHX34k0tfHs#v=onepage&q=(Wang+etal.%2C+2017&f=false)>
- Hudson, J. J., Dillon, P. J., & Somers, K. M. (2002). 'Long-term patterns in dissolved organic carbon in boreal lakes: the role of incident radiation, precipitation, air temperature, southern oscillation and acid deposition', *Hydrology and Earth System Sciences Discussions*, 7/3: 390–8.
- Kebede, E. W. (2009). *Hydrological Responses To Land Cover Changes In Gilgel Abay Catchment, Ethiopia*.

- Retrieved August 24, 2018, from
<https://webapps.itc.utwente.nl/librarywww/papers_2009/msc/wrem/ermiru.pdf>
- Kokkonen, T. S., Jakeman, A. J., Young, P. C., & Koivusalo, H. J. (2003). 'Predicting daily flows in ungauged catchments: model regionalization from catchment descriptors at the Coweeta Hydrologic Laboratory, North Carolina', *Hydrological Processes*, 17/11: 2219–38. John Wiley & Sons, Ltd. DOI: 10.1002/hyp.1329
- Krause, P., Boyle, D. P., & Bäse, F. (2005). *Comparison of different efficiency criteria for hydrological model assessment. Advances in Geosciences*, Vol. 5. Retrieved February 14, 2019, from <<https://www.adv-geosci.net/5/89/2005/adgeo-5-89-2005.pdf>>
- Landis, J. R., & Koch, G. G. (1977). 'The Measurement of Observer Agreement for Categorical Data', *Biometrics*, 33/1: 159. DOI: 10.2307/2529310
- Lillesand, T. M., Kiefer, R. W., & Chipman, J. W. (2014). *Remote sensing and image interpretation*.
- Mango, L. M., Melesse, A. M., McClain, M. E., Gann, D., & Setegn, S. G. (2011). 'Land use and climate change impacts on the hydrology of the upper Mara River Basin, Kenya: results of a modeling study to support better resource management', *Hydrology and Earth System Sciences*, 15/7: 2245–58. DOI: 10.5194/hess-15-2245-2011
- Marhaento, H. (2018). 'Attribution of changes in the water balance of a tropical catchment to land use change using the SWAT model'. *Effects of changes in land use and climate on water availability of a tropical catchment*, pp. 13–26. DOI: 10.3990/1.9789036544917
- Marhaento, H., Booij, M. J., Rientjes, T. H. M., & Hoekstra, A. Y. (2017). 'Attribution of changes in the water balance of a tropical catchment to land use change using the SWAT model', *Hydrological Processes*, 31/11: 2029–40. DOI: 10.1002/hyp.11167
- Marshall, L., Nott, D., & Sharma, A. (2005). 'Hydrological model selection: A Bayesian alternative', *Water Resources Research*, 41/10. John Wiley & Sons, Ltd. DOI: 10.1029/2004WR003719
- Mcintyre, N., Lee, H., Wheeler, H., Young, A., & Wagener, T. (2005). 'Ensemble predictions of runoff in ungauged catchments', DOI: 10.1029/2005WR004289
- Mekonnen, D. F., Duan, Z., Rientjes, T., & Disse, M. (2018). 'Analysis of combined and isolated effects of land-use and land-cover changes and climate change on the upper Blue Nile River basin's streamflow', *Hydrology and Earth System Sciences*, 22/12: 6187–207. DOI: 10.5194/hess-22-6187-2018
- Merz, R., & Blöschl, G. (2004). 'Regionalisation of catchment model parameters', *Journal of Hydrology*, 287/1–4: 95–123. Elsevier. DOI: 10.1016/J.JHYDROL.2003.09.028
- Meyer et.al. (1995). 'Past and Present Land Use and Land Cover in the U.S.A. - ScienceBase-Catalog' 1995. Retrieved August 21, 2018, from
<<https://www.sciencebase.gov/catalog/item/50578a5de4b01ad7e0281bcd>>
- Meyer, W. B. (1995). 'Past and present land use and land cover in the USA', *Consequences*, 1/1: 25–33.
- Mohamed, Y. A., Savenije, H. H. G., & Bastiaanssen, W. G. M. (2005). 'Hydroclimatology of the Nile: results from a regional climate model', 263–78. DOI: 10.5194/hess-9-263-2005
- Montanari, A., & Di Baldassarre, G. (2013). 'Data errors and hydrological modelling: The role of model structure to propagate observation uncertainty', *Advances in Water Resources*, 51: 498–504. Elsevier. DOI: 10.1016/J.ADVWATRES.2012.09.007
- Moriasi, D. N., J. G. Arnold, J. G., M. W. Van Liew, M. W. Van, R. L. Bingner, R. L., R. D. Harmel, R. D., & T. L. Veith, T. L. (2007). 'Model Evaluation Guidelines for Systematic Quantification of Accuracy in Watershed Simulations', *Transactions of the ASABE*, 50/3: 885–900. American Society of Agricultural and Biological Engineers. DOI: 10.13031/2013.23153
- Nash, J. E., & Sutcliffe, J. V. (1970). 'River flow forecasting through conceptual models part I — A discussion of principles', *Journal of Hydrology*, 10/3: 282–90. Elsevier. DOI: 10.1016/0022-1694(70)90255-6
- Neitsch. (2005). *Soil and Water Assessment Tool Theoretical Documentation Version 2005*. Retrieved August 22, 2018, from <<https://swat.tamu.edu/media/1292/SWAT2005theory.pdf>>
- Neitsch, S. L., Arnold, J. G., Kiniry, J. R., Srinivasan, R., & Williams, J. R. (2004). *SOIL AND WATER ASSESSMENT TOOL INPUT/OUTPUT FILE DOCUMENTATION VERSION 2005*. Retrieved February 20, 2019, from <<https://swat.tamu.edu/media/1291/SWAT2005io.pdf>>
- NMSA. (2001). *Federal Democratic Republic of Ethiopia Ministry of Water Resources National Meteorological Services Agency*. Retrieved February 16, 2019, from <<https://unfccc.int/resource/docs/natc/ethnc1.pdf>>
- Parajka, J., Merz, R., & Blöschl, G. (2005). *Hydrology and Earth System Sciences A comparison of regionalisation*

- methods for catchment model parameters. *Hydrology and Earth System Sciences*, Vol. 9. Retrieved February 21, 2019, from <www.copernicus.org/EGU/hess/hess/9/157/SRef-ID:1607-7938/hess/2005-9-157EuropeanGeosciencesUnion>
- Pokhrel. (2018). 'Impact of Land Use Change on Flow and Sediment Yields in the Khokana Outlet of the Bagmati River, Kathmandu, Nepal', *Hydrology*, 5/2: 22. Multidisciplinary Digital Publishing Institute. DOI: 10.3390/hydrology5020022
- Quilbé, R., Rousseau, A. N., Moquet, J.-S., Savary, S., Ricard, S., & Garbouj, M. S. (2008). 'Hydrological responses of a watershed to historical land use evolution and future land use scenarios under climate change conditions', *Hydrology and Earth System Sciences*, 12/1: 101–10. DOI: 10.5194/hess-12-101-2008
- Renner, M., Kleidon, A., & Porada, P. (2014). 'Estimates of the climatological land surface energy and water balance derived from maximum convective power', *Hydrology and Earth System Sciences*, 18/6: 2201–18. European Geosciences Union. DOI: 10.5194/hess-18-2201-2014
- Riebsame, W. E., Meyer, W. B., & Turner, B. L. (1994). 'Modeling land use and cover as part of global environmental change', *Climatic Change*, 28/1–2: 45–64. Kluwer Academic Publishers. DOI: 10.1007/BF01094100
- Rientjes, T. (2015). 'Hydrologic modelling for Intergated Water Resource', *Lecture notes for Module 9-10 surface water stream*.
- Rientjes, T. H. M., Haile, A. T., Kebede, E., Mannaerts, C. M. M., Habib, E., & Steenhuis, T. S. (2011a). 'Changes in land cover, rainfall and stream flow in Upper Gilgel Abbay catchment, Blue Nile basin – Ethiopia', *Hydrology and Earth System Sciences*, 15/6: 1979–89. DOI: 10.5194/hess-15-1979-2011
- Rientjes, T. H. M., Haile, A. T., Kebede, E., Mannaerts, C. M. M., Habib, E., & Steenhuis, T. S. (2011b). 'Hydrology and Earth System Sciences Changes in land cover, rainfall and stream flow in Upper Gilgel Abbay catchment, Blue Nile basin-Ethiopia', *Hydrol. Earth Syst. Sci*, 15. DOI: 10.5194/hess-15-1979-2011
- Rosenfield, G. H., & Fitzpatrick-Lins, K. (1986). 'A coefficient of agreement as a measure of thematic classification accuracy.', *Photogrammetric Engineering and Remote Sensing*, 52/2: 223–7.
- Setegn, S. G., Srinivasan, R., & Dargahi, B. (2008). 'Hydrological Modelling in the Lake Tana Basin, Ethiopia Using SWAT Model', *The Open Hydrology Journal*, 2/1: 49–62. DOI: 10.2174/1874378100802010049
- Smedema, L. K., & Rycroft, D. W. (1983). *Land drainage : planning and design of agricultural drainage systems*. Cornell University Press.
- Tegegne, G., Park, D. K., & Kim, Y.-O. (2017). 'Comparison of hydrological models for the assessment of water resources in a data-scarce region, the Upper Blue Nile River Basin', *Journal of Hydrology: Regional Studies*, 14: 49–66. Elsevier. DOI: 10.1016/J.EJRH.2017.10.002
- van den Tillaart, S. P. M., Booij, M. J., & Krol, M. S. (2013). 'Impact of uncertainties in discharge determination on the parameter estimation and performance of a hydrological model', *Hydrology Research*, 44/3: 454–66. IWA Publishing. DOI: 10.2166/nh.2012.147
- Tomer, M. D., & Schilling, K. E. (2009). 'A simple approach to distinguish land-use and climate-change effects on watershed hydrology', *Journal of Hydrology*, 376/1–2: 24–33. Elsevier. DOI: 10.1016/J.JHYDROL.2009.07.029
- Uhlenbrook, S., Mohamed, Y., & Gragne, A. S. (2010). 'Analyzing catchment behavior through catchment modeling in the Gilgel Abay, Upper Blue Nile River Basin, Ethiopia', *Hydrology and Earth System Sciences*, 14/10: 2153–65. DOI: 10.5194/hess-14-2153-2010
- White & Chaubey. (2005). *Sensitivity Analysis, Calibration, and Validation for a Multiste and Multivariable SWAT Model 1*. Retrieved August 22, 2018, from <https://engineering.purdue.edu/ecohydrology/Pubs/White_Chaubey_JAWRA_Oct05.pdf>
- Williams, J. R., & Hann, R. W. (1972). 'Hymo, A problem-oriented computer language for building hydrologic models', *Water Resources Research*, 8/1: 79–86. Wiley-Blackwell. DOI: 10.1029/WR008i001p00079
- Yalew, S. G. (2018). *Integrated Modeling of Land and Water Resources in Two African Catchments*. CRC Press. DOI: 10.1201/9780429489457
- Zheng. (2016). 'Assessment of the Spatial and Temporal Variations of Water Quality for Agricultural Lands with Crop Rotation in China by Using a HYPE Model', *International Journal of Environmental Research and Public Health*, 13/3: 336. DOI: 10.3390/ijerph13030336

Appendix:

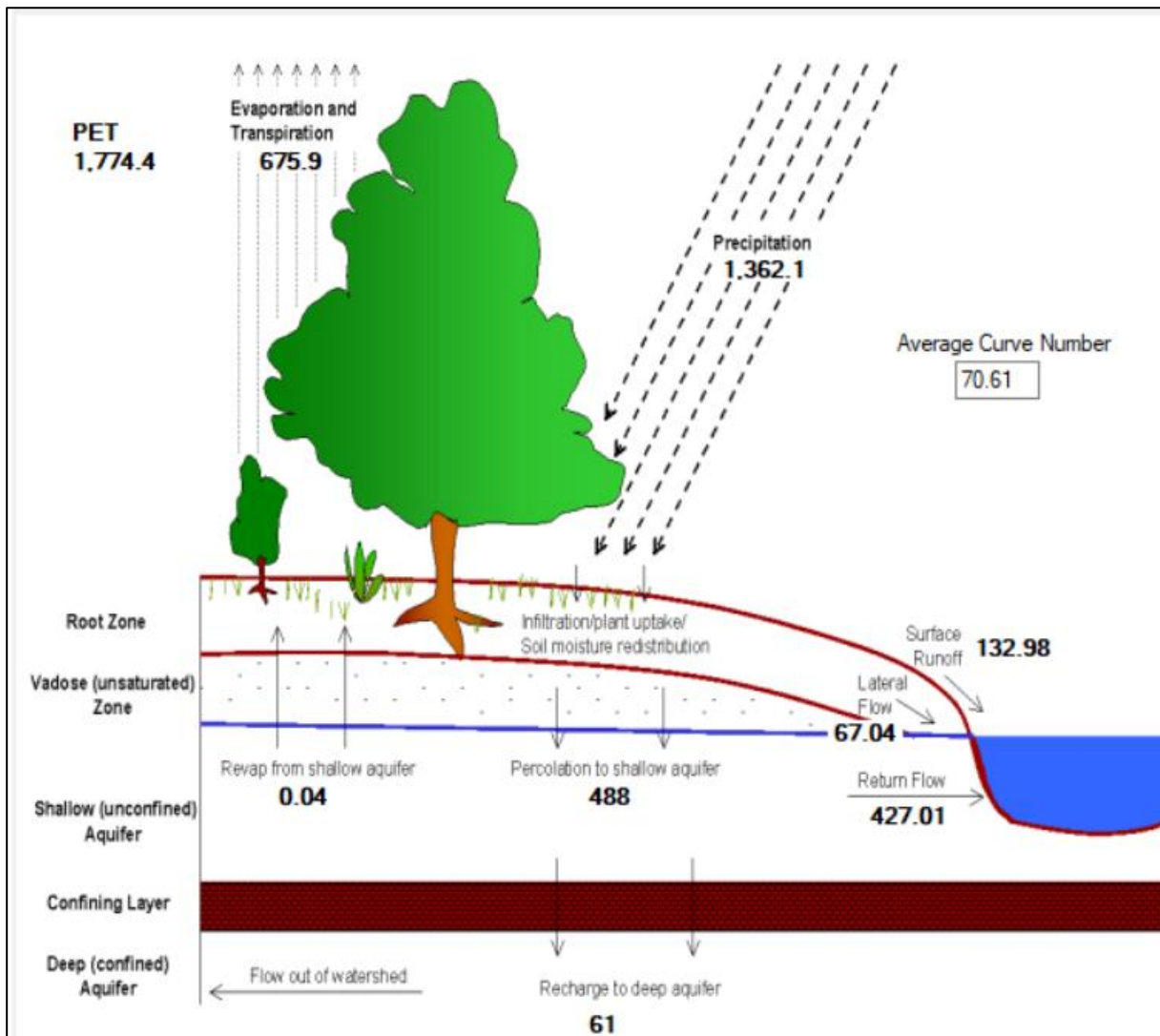


Figure 24: Representation of SWAT model for water balance

The figures below show daily rainfall of eight meteorological stations

Figure 25: Daily rainfall for each station

